AFRL-AFOSR-VA-TR-2020-0043

Explosive Ozonolysis Reactions for Combustion Control

Wenting Sun
GEORGIA TECH RESEARCH CORPORATION

11/22/2019
Final Report

Air Force Research Laboratory
AF Office Of Scientific Research (AFOSR)/ RTA1
Arlington, Virginia 22203
Air Force Materiel Command

DISTRIBUTION A: Distribution approved for public release.

REPORT DOCUMENTATION PAGE

Form Approved
OMB No. 0704-0188

1. REPORT DATE *(DD-MM-YYYY)*	2. REPORT TYPE	3. DATES COVERED *(From - To)*
20-05-2020	Final Performance	01 Sep 2016 to 31 Aug 2019

4. TITLE AND SUBTITLE
Explosive Ozonolysis Reactions for Combustion Control

5a. CONTRACT NUMBER

5b. GRANT NUMBER
FA9550-16-1-0441

5c. PROGRAM ELEMENT NUMBER
61102F

6. AUTHOR(S)
Wenting Sun

5d. PROJECT NUMBER

5e. TASK NUMBER

5f. WORK UNIT NUMBER

7. PERFORMING ORGANIZATION NAME(S) AND ADDRESS(ES)
GEORGIA TECH RESEARCH CORPORATION
505 10TH ST NW
ATLANTA, GA 30318-5775 US

8. PERFORMING ORGANIZATION REPORT NUMBER

9. SPONSORING/MONITORING AGENCY NAME(S) AND ADDRESS(ES)
AF Office of Scientific Research
875 N. Randolph St. Room 3112
Arlington, VA 22203

10. SPONSOR/MONITOR'S ACRONYM(S)
AFRL/AFOSR RTA1

11. SPONSOR/MONITOR'S REPORT NUMBER(S)
AFRL-AFOSR-VA-TR-2020-0043

12. DISTRIBUTION/AVAILABILITY STATEMENT
A DISTRIBUTION UNLIMITED: PB Public Release

13. SUPPLEMENTARY NOTES

14. ABSTRACT

This report summarizes the important activities and findings for AFOSR Grant FA9550-16-1-0441, 'YIP: Explosive Ozonolysis Reactions for Combustion Control' for the reporting period Sept. 1 2016 Aug. 31 2019. During this project, work has been focused on the study of 1) the effect of ozonolysis reaction introduced autoignition on flame dynamics at conditions with and without artificial turbulence generation; 2) CFD model construction for 2D simulation; 3) fundamental study of ozonolysis reactions in a flow reactor; 4) lifted flame experiments at steady state. We found that 1) ozonolyisis reaction occurs at room temperature therefore causing spontaneous/autoignition to dramatically change flame dynamics. Flame propagation speed of the order of 300 m/sec was observed with the assistance of autoignition; 2) turbulence significantly enhances mixing therefore ozonolysis reaction to accelerate autoignition; 3) the products of ozonolysis reactions of ethylene are dominantly formaldehyde (CH2O), hydrogen (H2), and some larger hydrocarbons. Ozonolyisis reaction scheme is extremely complicated. Photon Ionization Experiment allowed the detection of intermediate species and its evolution in terms of residence time. Some species are the first time to be measured in ozonolysis reactions; 4) In the lifted experiment, we demonstrated O3 could either increase or decrease the liftoff height depending on the ozone concentrations. As the ozone concentration changes, the controlling mechanism also changes. The results from this experimental platform provides good insights to flame dynamics in autoigniting environments which could occur in turbulent combustion. Formaldehyde (CH2O) PLIF confirmed the formation of CH2O in the mixing layer. These efforts are described in the following sections in accordance with the tasks breakdown.

15. SUBJECT TERMS
Combustion Chemistry, ozone, O3

16. SECURITY CLASSIFICATION OF:			17. LIMITATION OF ABSTRACT	18. NUMBER OF PAGES	19a. NAME OF RESPONSIBLE PERSON
a. REPORT	b. ABSTRACT	c. THIS PAGE			LI, CHIPING
Unclassified	Unclassified	Unclassified	UU		19b. TELEPHONE NUMBER *(Include area code)* 703-696-8574

Standard Form 298 (Rev. 8/98)
Prescribed by ANSI Std. Z39.18

(YIP) Explosive Ozonolysis Reactions for Combustion Control

Final Report

AFOSR Project: FA9550-16-1-0441

Submitted by:

Georgia Institute of Technology
Atlanta, GA 30332

Principal Investigator: Wenting Sun

School of Aerospace Engineering
Georgia Institute of Technology
Atlanta, GA 30332
Phone: (404) 894-0524
FAX: (404) 894-2760
Email: wenting.sun@aerospace.gatech.edu

Prepared for
Air Force Office of Scientific Research

Period of Performance
(Sept. 1 2016 – Aug. 31 2019)

Submitted on
Nov. 20, 2019
DUNS Number: 09-739-4084

Summary: This report summarizes the important activities and findings for AFOSR Grant FA9550-16-1-0441, "YIP: Explosive Ozonolysis Reactions for Combustion Control" for the reporting period Sept. 1 2016 – Aug. 31 2019. During this project, work has been focused on the study of 1) the effect of ozonolysis reaction introduced autoignition on flame dynamics at conditions ***with and without artificial turbulence generation***; 2) CFD model construction for 2D simulation; 3) fundamental study of ozonolysis reactions in a flow reactor; 4) lifted flame experiments at steady state. We found that 1) ozonolysis reaction occurs at room temperature therefore causing spontaneous autoignition to dramatically change flame dynamics. Flame propagation speed of the order of 300 m/sec was observed with the assistance of autoignition; 2) turbulence significantly enhances mixing therefore ozonolysis reaction to accelerate autoignition; 3) the products of ozonolysis reactions of ethylene are dominantly formaldehyde (CH_2O), hydrogen (H_2), and some larger hydrocarbons. Ozonolysis reaction scheme is extremely complicated. Tunable photoionization technique allowed the detection of reactive intermediate species and its evolution in terms of residence time. Some species are the first time to be measured in ozonolysis reaction scheme; 4) In the lifted flame experiment, we demonstrated the addition of O_3 could either increase or decrease the liftoff height depending on the initial liftoff height at O_3 free condition. As the initial liftoff height differs, the controlling mechanism also changes. The results from this experimental platform provide good insights to flame dynamics in autoigniting environments which could occur in turbulent combustion. Formaldehyde (CH_2O) PLIF confirmed the formation of CH_2O in the mixing layer. These efforts are described in the following sections in accordance with the tasks breakdown.

1. **Task 1 – Study of ozonolysis reactions and development of the ozonolysis reaction mechanism**

The first task of this project is to investigate ozonolysis reactions between ozone (O_3) and ethylene (C_2H_4) in combustion environment. In this project, we have designed and fabricated a novel flow reactor allowing fast mixing and conducted measurement of products from ozonolysis reaction. We used tunable photoionization to quantify unstable products from ozonolysis reaction through a collaboration with the National Synchrotron Radiation Lab in the University of Science and Technology of China to use the synchrotron radiation and molecular beam mass spectrometer (MBMS) resources there. The integration of tunable photoionization and MBMS system allows the quantification of many short lifespan species produced from ozonolysis reactions.

In this project, we designed and fabricated a novel flow reactor for the study of ozonolysis reaction. The key in the design is fast mixing between fuel (C_2H_4) and O_3. Because O_3 and C_2H_4 reacts very quickly at room temperature, the flow reactor must run at non-premixed mode and achieve very fast mixing in the inlet region of the reactor. In the design of the flow reactor, FLUENT was employed to design the mixing section and model flow field, uniformity of the reactants downstream. The design and modeling of the flow reactor are shown in Fig. 1 and Fig. 2. In order to enhance mixing, stainless steel muffler is used for fuel injection. It can be seen that current design of flow reactor can achieve very fast online mixing before the inlet of the reactor and the distribution of reactants is reasonably uniform downstream of the reactor. Therefore, it allows reliable sampling and optical measurement of both reactants and products inside the reactor.

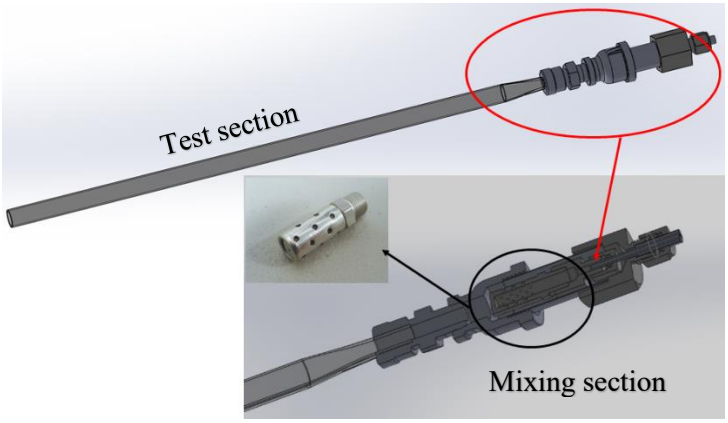

Fig. 1 The design of plug flow reactor (PFR)

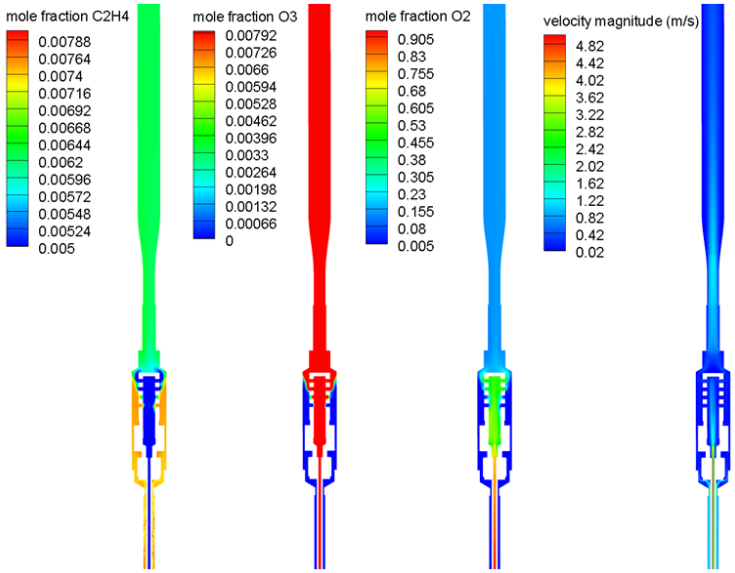

Fig. 2 Numerical results from FLUENT. Steady state, plotting on the middle cross section plane for mole fraction of C_2H_4; mole fraction of O_3; mole fraction of O_2 and velocity magnitude.

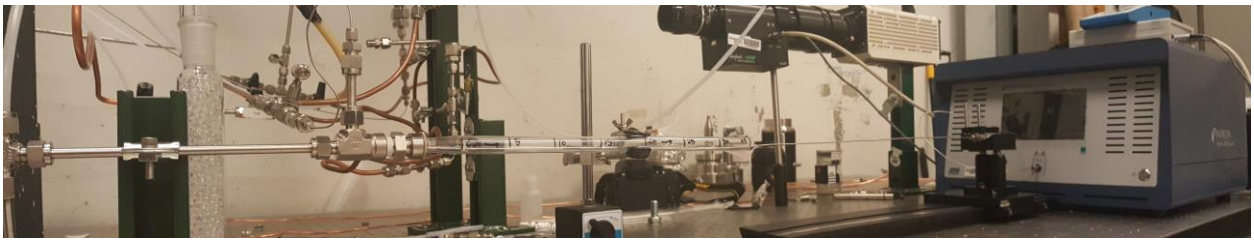

Fig. 3 Direct photograph of experimental setup of flow reactor

Figure 3 shows the direct photograph of the flow reactor setup. At first, no O_3 is generated from O_2. Samples are taken at 0 cm, 15 cm and 25 cm in PFR test section to test the mixing and to record the original species before O_3 addition. The measured concentrations from GC are 7819 ppm for C_2H_4 and 30,903 ppm for O_2 diluted by N_2 with overall equivalence ratio $\phi = 0.9983$ which is near stoichiometry. Then different amounts of O_3 are generated by the ozone generator from the O_2 stream, such that the potential effects of equivalence ratio on ozonolysis pathways can be

investigated. According to existing reference [1, 2], CH_2O, CO, H_2, CO_2 and H_2O are all possible in the products of C_2H_4 ozonolysis reactions. To check the existence of these species, we compared the chromatograms from non-ozone case with the O_3 addition cases, at different locations in PFR test section with 2100 ppm O_3 concentrations. GC measurement is shown in Fig. 4 and it shows that CH_2O (2000 ppm level) is one of the major ozonolysis products of C_2H_4. GC measurement also identified large amount of H_2 (200 ppm level) production beside CO_2 and H_2O. The ratio between CH_2O and H_2 is near 10, strongly differentiating from prediction using existing kinetic model developed by atmospheric chemistry society. It is worthy to note that onboard H_2 and CH_2O production has broad application.

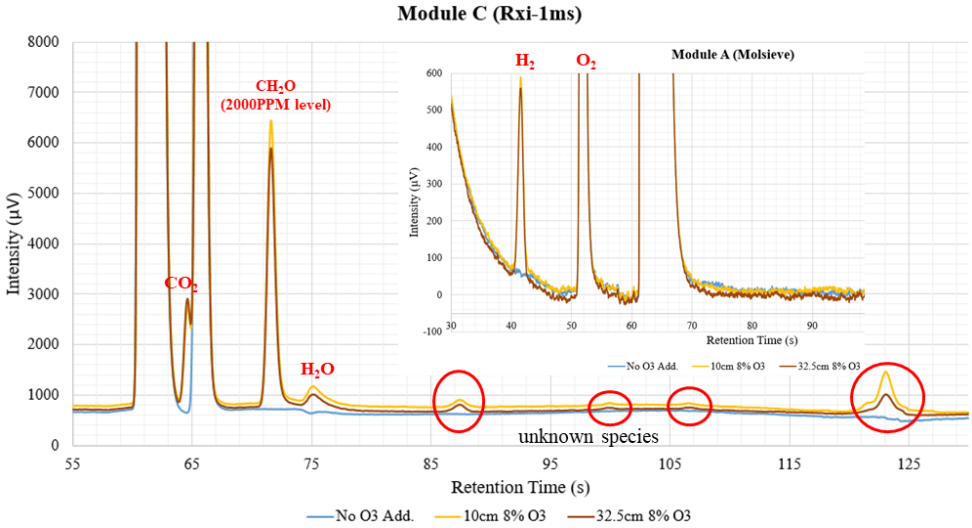

Fig. 4 GC measurement

We also observed that there were several peaks at long retention times. Those are supposed to be relatively large hydrocarbons (>C_2), since large molecules tend to pass through columns in GC slower than small molecules, which give them a longer retention time.

To further understand the scheme of ozonolysis reaction, synchrotron radiation based photoionization MBMS (Molecular Beam Mass Spectrometer) experiments were conducted. Nearly 50 species were detected including very large hydrocarbons from C_2H_4/O_3 ozonolysis reactions at atmospheric pressure and room temperature. The main purpose of this study is to identify products and intermediates in C_2H_4 ozonolysis system, therefore, photoionization efficiency (PIE) curves are recorded from 8.3-11.8 eV with 0.02 eV/step and 200 s/step at $C_2H_4/O_2/O_3/Ar$=18109/94056/1920/balance, (ppm), noted as case (A). The reactant C_2H_4 is nearly 10 times excess compared with O_3 to ensure that ozonolysis is dominant in this chemical system. Additionally, another two subsidiary experiments are designed with different initial concentrations: extremely low reactants concentrations noted as case (B), $C_2H_4/O_2/O_3/Ar$=101/875/13/balance, (ppm); and the other one is O_3 excessive high reactants concentrations case (C), $C_2H_4/O_2/O_3/Ar$=727/117185/7083/balance, (ppm). Those two additional experiments are mean to assist in identifying and confirming unknown species. The PIE curves under condition case (C) are scanned from 9.10-11.22 eV, with 0.04 eV/step and 200 s/step, while conditions of case (A) and case (B) share the same setup of PIE curves recording.

A relatively high photon energy was used to only present major products, as shown in Fig. 5. With photon energy of 14.49 eV, all products were ionized even permanent gases. In addition to those well-known major products, many other MS peaks showed up and some had mass-to-charge ratios (m/z) even larger than 100. Stable products may have relatively high ionization potentials, and it was very possible that some other large molecules in products would photodissociate and gave away ions with exactly same m/z, thus covered the potential products signal. The extremely low reactants concentrations, i.e. case (B), experiments were designed to suppress such fragmentation caused by photodissociating ionization, so that products and intermediates with low abundance can be detected without interference. Some PIE curves of selected major products were presented in Fig. 6(a)-(d), vertical axis represents relative photon signal intensity of random unit.

By comparing the threshold photoionization energy obtained from PIE curve experimentally, and evaluated ionization energy from NIST database [3], unknown species at given m/z can be identified. For some common species, their photoionization cross section (PICS)as a function of photon energy were measured and can be used for further confirmation by line shape matching, which are plotted as red curves in Fig. 6. Fig. 6(a) shows the existence of C_2H_2 as one of products, which was not detected by any others before. However, no strong signal of C_2H_2 was seen at O_3 excess case (C). This might be due to the higher abundance of vinyl radicals in the system with concentration case (A) compared with case (C). In Fig. 6(b), PIE curves from both low and high concentrations experiments are given, and methanol (CH_3OH) was confirmed by the PIE from case (B), which has good agreement with PICS curve from Ref. [4]. The ionization signal appeared around 10.4eV in Case (A) was likely to be $[CH_2OH_2]^+$ fragment from the photodissociation of hydroxy-acetaldehyde ($HOCH_2CHO$) [5], which was also confirmed as a minor products. Although species with molecular formulas C_2H_6O and CH_2O_2 are not isomers, the difference between their accurate molecular weights is within 0.038, which could not be resolved by the current RTOF mass spectroscopy. As shown in Fig. 6(d) for PIE curve of $m/z \approx 46$, both ethanol (C_2H_5OH) and formic acid (HCOOH) were identified.

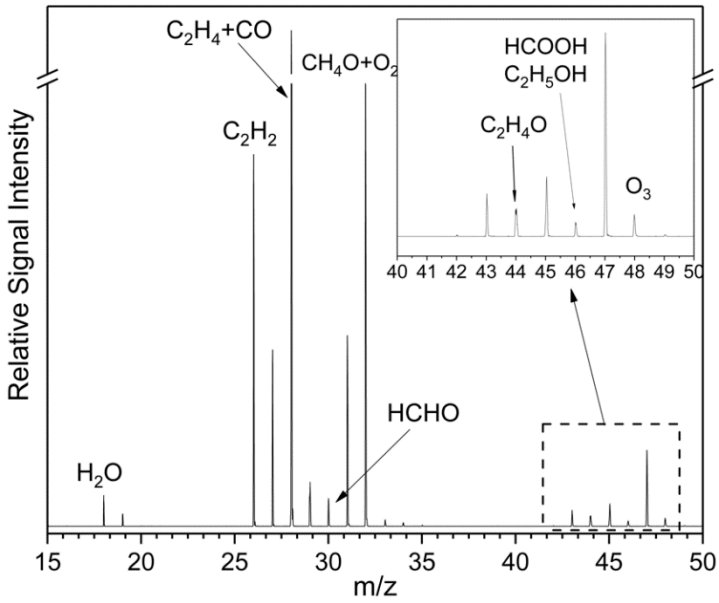

Figure 5. Mass spectroscopy recorded at photon energy 14.49 eV with resident time in PFR approximately 2 s and sampling duration 60 s

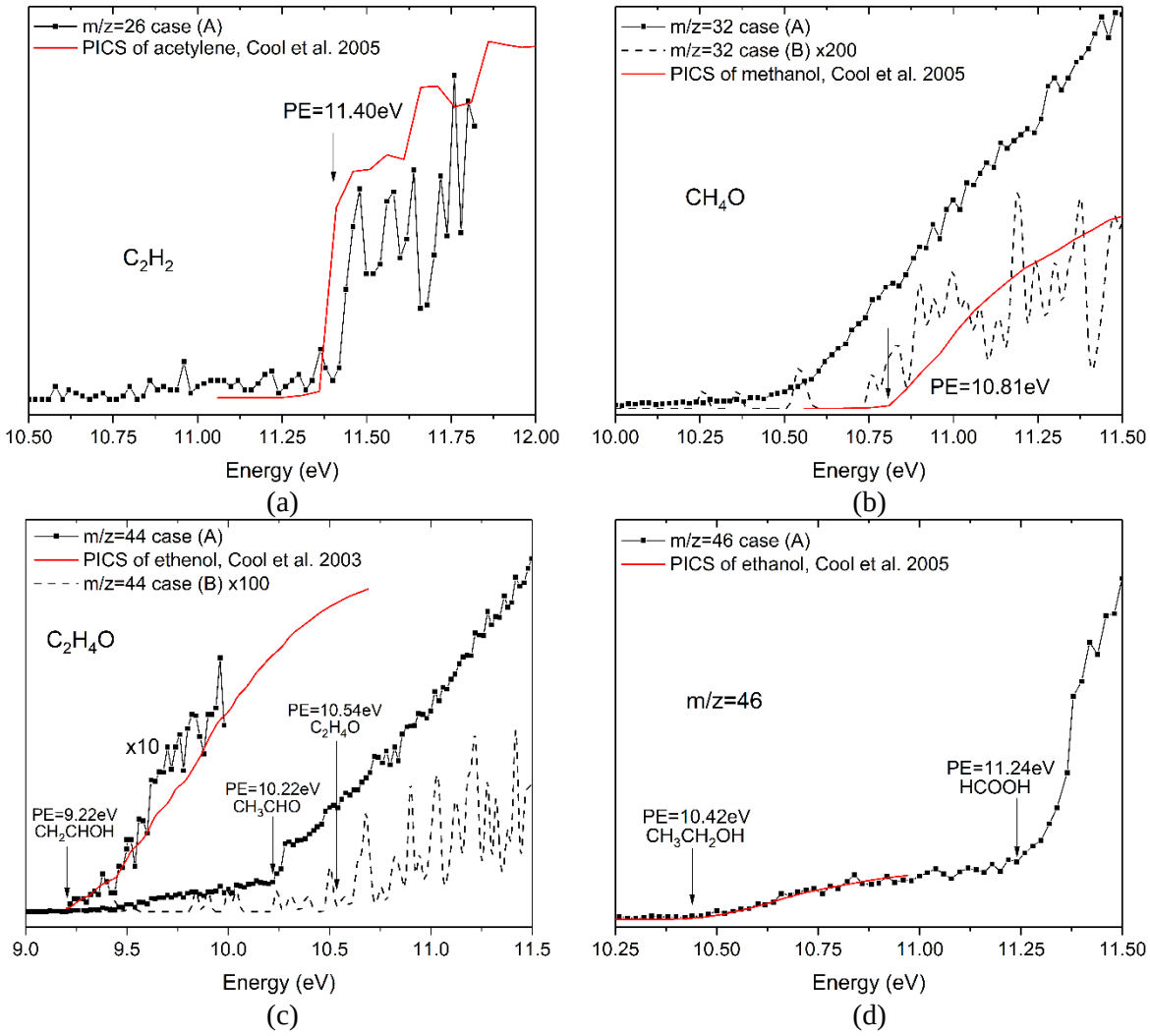

Figure 6. PIE curves of selected major products (a) C_2H_2, PICS of acetylene [4]; (b) CH_4O, PICS of methanol [4]; (c) C_2H_4O, PICS of ethenol [6]; (d) m/z=46, PICS of ethanol [4]

PIE curve of m/z=60 with molecular formula $C_2H_4O_2$ and m/z=76 $C_2H_4O_3$ are shown in Fig. 7. Three $C_2H_4O_2$ isomers have been identified so far, by comparing the calculated adiabatic ionization energy (AIE) with experiments. Hydroxy-acetaldehyde, i.e. $HOCH_2CHO$, was identified as a minor products, which agreed with the results shown in Ref. [7], and it will photodissociate at photon energy around 10.4 eV and release $[CH_2OH_2]^+$. The AIE of 1,2,4-trioxolane (an isomer of $C_2H_4O_3$) also known as the SOZ, is given in Ref. [7] as 9.68eV, which matches the experimental result of 9.70 eV as shown in Fig. 7(b). The SOZ yields from the recombination of sCI and formaldehyde as proposed by Criegee [2]. However, no report has been given regarding its existence in gas phase reactions until Womack et al. [8] did the experiment with relatively high reactants concentrations using fast-sampling Fourier transform microwave spectroscopy.

Some simple hydroperoxides and peroxy radicals are believed being detected and identified in this C_2H_4 ozonolysis chemical system as intermediates. Until now, detected m/z signals and

corresponding possible species are, HO_2 (m/z=33), H_2O_2 (m/z=34), CH_3OO (m/z=47), CH_3OOH (m/z=48), C_2H_2OO (m/z=58), C_2H_3OO (m/z=59), C_2H_3OOH (m/z=60), C_2H_5OO (m/z=61), C_2H_5OOH (m/z=62). Many of those peroxy radicals and molecules are important intermediates in widely existed low temperature fuel oxidation and playing critical roles in autoignition process [9]. However, it is nearly impossible to see them at atmospheric temperature regime, i.e. around 300 K, due to their high reactivity and lack of chain branching agents, for instance, H, OH, HCO, etc. The PIE curves of some confirmed peroxy species are presented in Fig. 8, in which PIE curves recorded under O_3 excess condition, i.e. case (C), are plotted with the ones from C_2H_4 excess case, i.e. case (A), for comparison purpose. The AIE of methyl-hydroperoxide is calculated using CBS-APNO method as 9.83 eV which is identical to the work of Rousso et al. [7], and matches the 9.82 eV by experiments. The calculated AIE of vinyl-peroxy radical C_2H_3OO is 9.80 eV that can match the 9.90 eV within permissible error 0.1 eV.

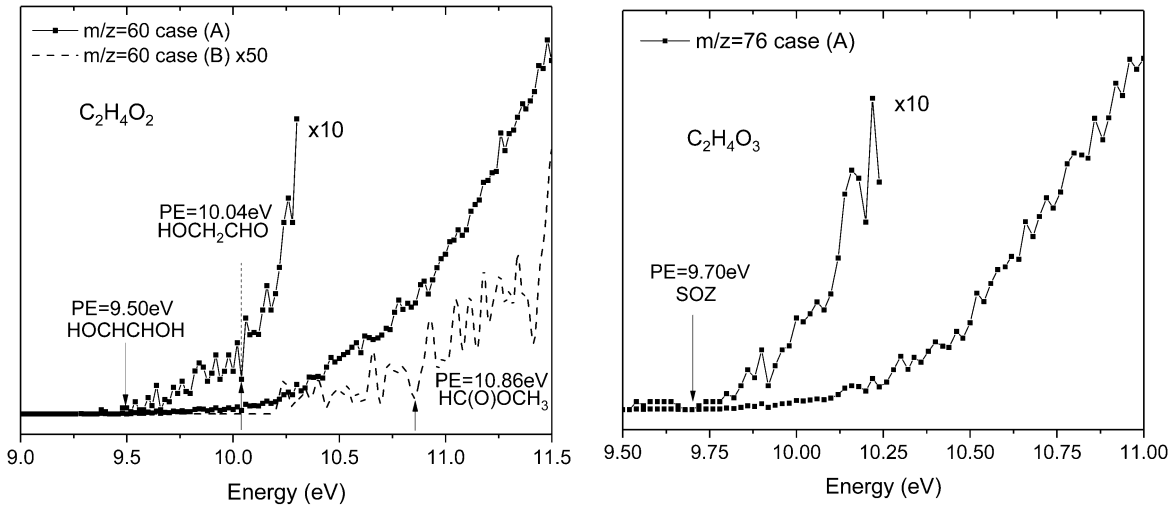

Figure 7. PIE curves of (a) $C_2H_4O_2$ and identified isomers; (b) $C_2H_4O_3$, 1,2,4-trioxolane

Ethyl-peroxy radical is also detected in our experiments and its PIE curve is shown in Fig. 9. The calculated AIE of ethyl-peroxy radical is 9.49 eV, which is very close to the value 9.48 eV calculated by Meloni et al. [10]. As shown in Fig. 9(a), an obvious rise can be noticed on the PIE curve of m/z=61 around 9.46 eV which matches the calculated AIE. However, in the work of [10], no determinant $C_2H_5OO^+$ is detected even in the specifically designed C_2H_5+O_2 environment, but rather an increment in $C_2H_5^+$ signal starts from energy around 10.0 eV due to photodissociation of C_2H_5OO. In Fig. 9(b), the PIE curve of m/z=29 C_2H_5 is presented and the threshold around 10-10.25 eV is consistent with the observation in Ref. [10]. Those two evidences strongly indicate the species with m/z=61 is the ethyl-peroxy radical C_2H_5OO. Nevertheless, we did not see certain evidence for the existence of methyl-peroxy radical CH_3OO and ethyl-hydroperoxide C_2H_5OOH, the later one has been reported by Rousso et al. [7] in a similar work conducted using a JSR as reactor instead. All identified products and intermediates in this work are summarized in Table 1.

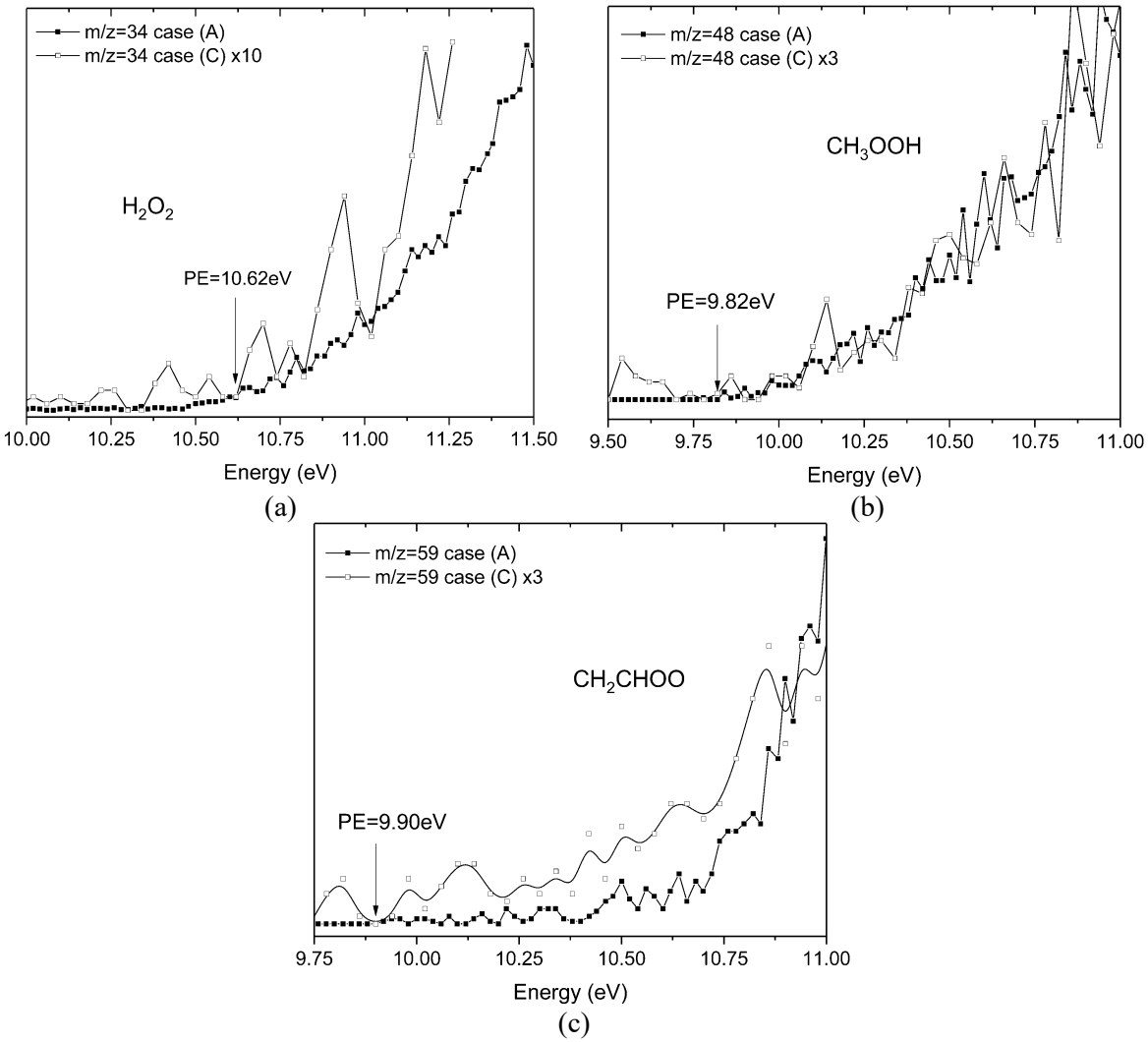

Figure 8. Some identified hydroperoxides and peroxy radical (a) H_2O_2; (b) CH_3OOH; (c) C_2H_3OO

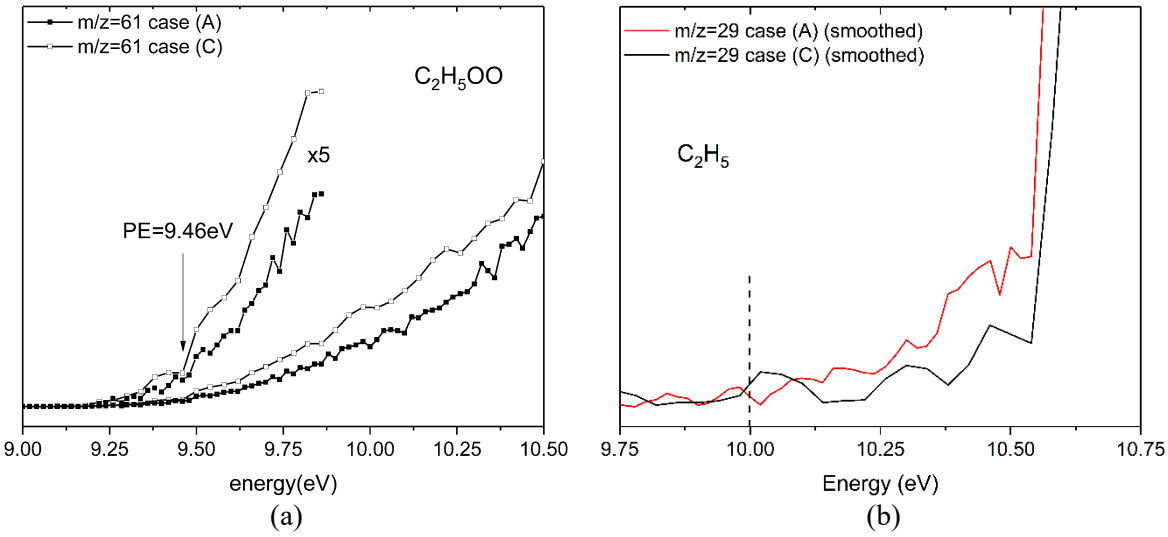

Figure 9. PIE curves of ethyl-peroxy and corresponding fragment ethyl radical (a) $C_2H_5O_2$; (b) C_2H_5

It is very likely that the formation of those hydroperoxides and peroxyl radicals in the ozonolysis system shares the same kinetic pathways as the traditional low temperature oxidation procedure described in [9]. The peroxy species formation could potentially start with chain propagating reactions $C_2H_4+H+M \rightarrow C_2H_5+M$, $C_2H_4+HCO \rightarrow C_2H_5+CO$, $C_2H_4+OH \rightarrow C_2H_3+H_2O$, etc., since both H, OH and HCO radicals are direct products from ozonolysis reaction as proposed by Criegee [2], then the alkyl and alkenyl radicals would rapidly combine with abundant O_2 and yield to peroxy radicals and hydroperoxides. With high concentrations of C_2H_4 and O_3 as reactants, those chain branching agents can be released with extremely high rate that gives possibility to peroxy radical formation and thus accumulation. It is reasonable to extrapolate that in this C_2 based hydrocarbon/oxidizer system, few methyl radicals would be generated and thus few CH_3OO radical as well, though no experimental evidence has been presented yet.

Table 1. Summarization of detected species by photoionization and MBMS in this work.
Species with * are species detected as products of C_2H_4 ozonolysis for the first time

m/z	Formula	Species name	Expt. (eV)	Theoretical AIE (eV)
26	C_2H_2	Acetylene*	11.40	11.40±0.002 [3]
32	CH_4O	Methanol	10.81	10.84±0.01 [3]
34	H_2O_2	Hydrogen peroxide	10.62	10.58±0.04 [3]
42	C_2H_2O	Ketene	9.62	9.617±0.003 [3]
44	C_2H_4O	Ethenol	9.22	9.18 [11]
		Acetaldehyde	10.22	10.229 [3]
		Ethylene oxide	10.54	10.56±0.01[3]
46	CH_2O_2	Formic acid	11.24	11.33±0.01 [3]
46	C_2H_6O	Ethanol*	10.42	10.48±0.07 [3]
48	CH_4O_2	Methyl-hydroperoxide	9.82	9.83
59	$C_2H_3O_2$	Vinyl-peroxyl radical*	9.90	9.80
60	$C_2H_4O_2$	Hydroxy-acetaldehyde	10.04	9.84-10.05 [7]
		Ethen-1,2-diol*	9.50	9.50
		Methyl formate*	10.86	10.835 [3]
61	$C_2H_5O_2$	Ethyl-peroxyl radical*	9.46	9.49 /9.48 [10]
76	$C_2H_4O_3$	1,2,4-Trioxolane	9.70	9.68 [7]

2. Task 2 – Investigation of ozonolysis induced autoignition and autoignition sustained C_2H_4 diffusion jet flame

This task is to investigate the effect of autoignition kernels introduced by room temperature ozonolysis reactions on flame dynamics. Specifically, the focus is that how autoignition kernel was formed in such an autoigniting environment, and how the autoignition kernel affects subsequent flame propagations. The spontaneous reactions in the reacting layer are studied with and without artificial turbulence generated using metal mesh.

2.1. Experimental and Computational Method

Table 2 summarizes the reaction rate constants between ozone and some typical hydrocarbons based on existing references. As shown in the table, ozone reacts with unsaturated hydrocarbons (ozonolysis reactions) extremely fast even at room temperature. So, the experiment has to be run at non-premixed mode to avoid fast mixing/reaction therefore heat loss to ambient.

Table 2. Ozonolysis reactions rates constants, *k*, at room temperature and pressure

		k (cm^3/mole-s)	Reference
Alkanes	CH_4	0.99	[12]
	C_2H_6	8.95	[13]
	C_3H_8	4.19	[13]
	C_4H_{10}	6.05	[12]
Unsaturated Hydrocarbons	C_2H_4	1.12×10^6	[14]
	C_3H_6	6.29×10^6	[15]
	iso-C_4H_8	7.13×10^6	[16]
	1-C_4H_8	5.82×10^6	[16]

In this study, a non-premixed co-flow configuration is adopted, as illustrated in Fig. 10. The fuel (C_2H_4) is the center jet and the oxidizer ($O_2/O_3/N_2$) is the co-flow jet. The exit of the nozzle tube supplying the fuel has an outer diameter (OD) of 0.317 cm, and inner diameter (ID) of 0.176 cm. To block the dilution effects of the ambient air, the reactants jets are surrounded by a quartz tube, which has a length of 30 cm, ID of 0.787 cm and OD of 1.27 cm. N_2, O_2 (99.994% purity), and C_2H_4 are sent through a bank of calibrated flow controllers. O_2 is sent through an O_3 generator (Ozone solution, TG-40, during data acquisition the fluctuation of O_3 concentration is within 10%) to be partially ozonized. An O_3 monitor (Teledyne Instruments, Model 454, accuracy ±130 ppm) is connected downstream of the O_3 generator to measure O_3 concentration. N_2, O_2, and O_3 are mixed (as the oxidizer stream) and sent to the burner. A high-speed camera (NAC, Memrecam GX-3) is used to record the intensity of the chemiluminescence from the flames. Filtered chemiluminescence at specific range of wavelength is also recorded with an intensifier (Lambert Instruments, HiCATT) and one of two optics bandpass filters, centered at 430 and 310 nm, respectively. Chemiluminescence from OH passes the one centered at 310 nm, and the signal from CH and CH_2O can pass the filter centered at 430 nm. The experiments are conducted at room temperature (~300 K) and pressure (~1 atm) conditions. The O_3 generator applies high-voltage pulse (5k-30k Hz) to convert O_2 to O_3. To minimize this unsteadiness effect, a mixing buffer is added between the O_3 generator and the O_3 monitor. This stainless-steel buffer has a volume of approximately 0.3 liter and is full of glass beads (diameter of 6.35 mm) to let O_2/O_3 well mixed before reaching the burner. During the experiment, initially the oxidizer and O_3 generator are turned on but the fuel stream turned off. At least 30 seconds are given to let the generation of O_3 reaches steady state. Then, fuel is turned on, and autoignition may occur, which will be recorded using the camera. After each experiment, the burner will be cleaned and cooled.

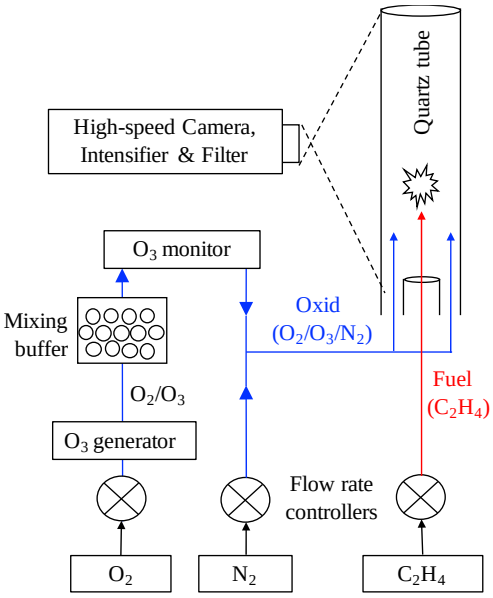

Fig. 10 Schematic of the experimental setup

The simulations in present work are conducted using ANSYS CHEMKIN software [17-19] for 1D model, and FLUENT software [20] for 3D model. For 1D model, the chemistry kinetics model is USC Mech II [21] combined with O_3 sub-mechanisms [22]. Specifically, the following ozonolysis reactions are assumed for C_2H_4 based on references:

$$C_2H_4+O_3=CH_2O+OH+HCO$$
$$C_2H_4+O_3=CH_2O+2H+CO_2$$
$$C_2H_4+O_3=CH_2O+H_2+CO_2$$
$$C_2H_4+O_3=CH_2O+H_2O+CO$$

These ozonolysis pathways share the same Arrhenius rates due to lack of detailed kinetic information, i.e.,

$$k = Ae^{-E/(RT)}$$

where R is the universal gas constant, T is the temperature, $A = 1.8\times10^9$ cm^3/mole-s-K is the pre-exponential factor, and $E = 5226$ cal/mole is the activation energy, based on [14]. For the 3D model, to reduce the computational cost, a 5-step mechanism is proposed, with the following Arrhenius parameters optimized using a genetic algorithm [23]. The validation results of this mechanism will be provided later.

	A	*E*
$C_2H_4 + O_3 => CH_2O + CO_2 + H_2$	7.226E+09	5227
$C_2H_4 + O_2 => 2\ CO + 2\ H_2$	1.166E+14	42408
$CH_2O => CO + H_2$	1.549E+10	16691
$H_2 + 0.5\ O_2 <=> H_2O$	6.637E+09	4972
$CO + 0.5\ O_2 <=> CO_2$	3.816E+08	23222

The autoignition and subsequent flame dynamics are investigated at the following flow conditions. The ratio of N atoms and O atoms (including these in O_2 and O_3) in the oxidizer jet is N/O = 0.28.

This value is lower than that in air to allow autoignition at the room temperature. The overall equivalence ratio (calculated using the number of C, H, and atoms in the well-mixed reactants) is ϕ = 0.4. 7.7% of O_2 is converted to O_3 and this corresponds (the mole fraction of O_3 in total reactants is 3.7%). The adiabatic 1D laminar flame speed, S_L, at such condition obtained using PREMIX [17] model is of the order of 1 m/s. The area-averaged velocity, U_0, defined as the ratio of the total flow rate of the reactants and the cross-section area of the quartz tube, is varied from 1.5 to 4 m/s. This corresponds to Reynolds number from 753 to 2008 based on the ID of the quartz tube. The autoignition kernel may propagate back, blow off, or interact with other autoignition kernels. These different phenomena can be observed (via the high-speed camera images) from a single experimental test within several seconds. Examples are discussed in detail below.

2.2. Experimental Observations

Through the experiments, different phenomena were observed including: multi-autoignition kernels, impulsive flash back, and ultra-fast flash back. The first phenomenon observed is the coexistence of multiple autoignition kernels, as shown in Fig. 11. At t = 0 ms, the first autoignition kernel (kernel-1 in Fig. 11) is generated at approximately 18 cm downstream of the burner exit. This is reasonably consistent with the simulation results using the PLUG [18] model (with the difference being due, presumably, to the time for mixing), which predicts the autoignition occurs at 14.5 cm downstream of the burner exit. This kernel then grows and propagates upstream. At t = 0.5ms, two new autoignition kernels (kernel-2 and kernel-3 in Fig. 11) are generated at approximately 1.3 cm upstream of the main flame front. Subsequently, these two autoignition kernels expands rapidly and merge with the main flame zone at t = 0.83 ms. The last autoignition kernel (kernel-4) is observed at t = 1.0 ms, upstream of the main flame front, and then it merges with the main flame.

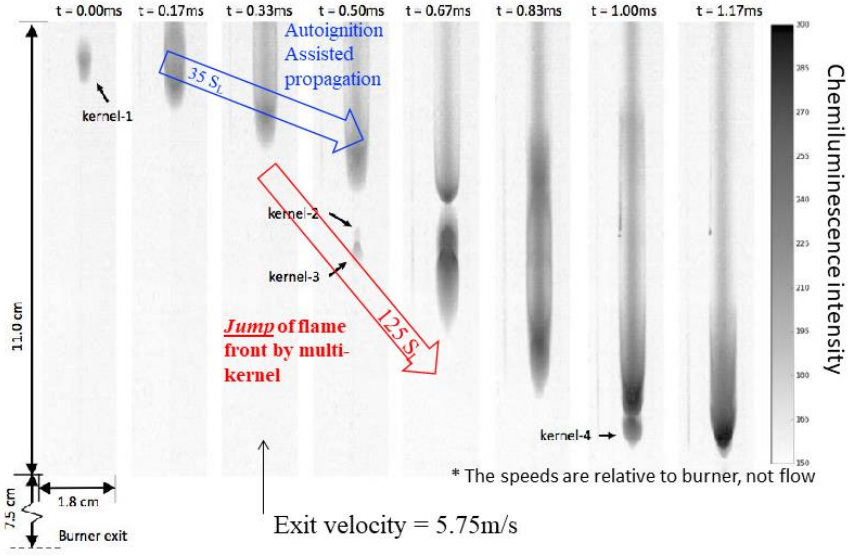

Fig. 11 Coexistence of multiple autoignition kernels

Several different flame dynamics may exist within the 1.17-ms timeframe illustrated in Fig. 11. The "propagation" of the leading edge of kernel-1 is at a very high speed of approximately 46 m/s from t = 0 to 0.33 ms. This is approximately 35 times S_L given by the PREMIX [17] model. It is conceivable that the propagation mechanism here is not exactly the same as with conventional flame propagation. Instead, autoignition may play an important role. This "propagation" with

much higher speed is referred to as the "autoignition-assisted propagation." The coexistence of multiple autoignition kernels makes the flame front "propagate" much faster. The generation of kernel-2 and kernel-3 at t = 0.5ms effectively moves the location of the main flame leading edge upstream. As a result, the "propagation" speed of the flame leading edge from t = 0.33 ms to 0.5 ms is approximately 162 m/s (location of flame front changed by 2.7 cm within 0.17 ms). This autoignition-based mechanism is, of course, very different than the conventional propagation mechanism. The latter is controlled by diffusion and can only stabilize the flame at relatively low flow velocity. In contrast, autoignition kernels are generated independently. Therefore, the propagation speed of autoignition-assisted flame could be referred to as a phase velocity. As long as the residence time is sufficiently long and heat loss is minimized, it is possible for a new autoignition kernel to be generated upstream of the existing flame zone, such as kernel-2 to kernel-4. This effectively "moves" the flame's leading edge upstream, therefore making it possible for flame to stabilize at high flow velocity.

The second phenomenon is referred as "impulsive flashback." Different flame stabilization mechanisms are suspected to coexist in this example. As illustrated in Fig. 12, the combustion zone is not moving upstream monotonically. The combustion zone is moving downstream at the moments labeled as "Type-I" but moving upstream at the moments labeled as "Type-II." Moving downstream implies the flame stabilization mechanism at these moments cannot sustain the flame at the original positions. The cone flame structure at t = 0.5 and 2.0 ms are similar to conventional Bunsen flames, suggesting the conventional flame propagation is the dominant flame stabilization mechanism at these moments. The ratio of the local flow velocity and flame propagation speed estimated from the cone structure at t = 2.0 ms, assuming it is a Bunsen flame, is 4.5. This is similar to the ratio of the inlet flow velocity, 5.75 m/s, to that S_L = 1.3 m/s, which further supports the idea that the flame stabilization mechanism at this moment is dominated by diffusion (as a conventional flame propagation mechanism). However, the conventional mechanism is not dominant when the combustion is moving upstream. In contrast to Type-I, no clear flame fronts are observed for the Type-II flames, and they are moving upstream at a speed of approximately 50 m/s. These features make Type-II flame fronts more similar to the "autoignition-assisted propagation" (illustrated in Fig. 11 during t = 0~0.33 ms), where the flame fronts are blurred and the propagation speed is of the similar order (46 m/s)

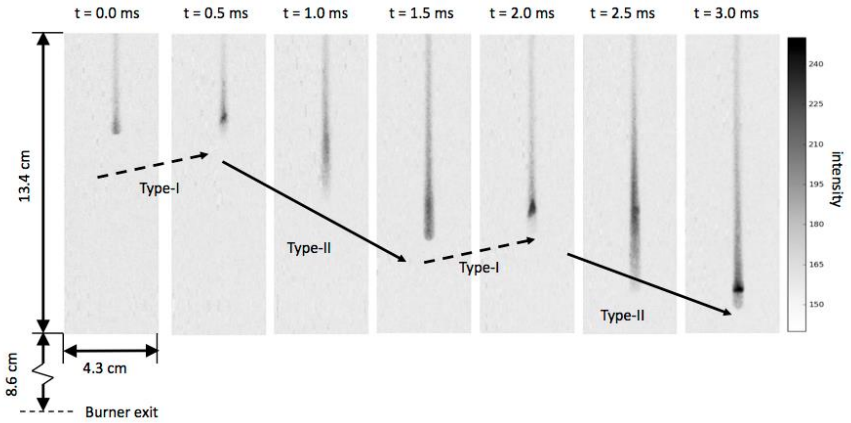

Fig. 12 Impulsive flashback

The third phenomenon is referred to as "ultra-fast flashback," as illustrated in Fig. 13. At t = 0 ms, almost no chemiluminescence can be detected, except a very weak combustion zone far downstream. However, at t = 0.5 ms, strong signal is observed, and the flame appears to flashback. This propagation speed is approximately 330 m/s. Then, the reactants are consumed rapidly. The underlying mechanism for this ultra-fast flashback deserves further investigations. However, as the possibility of the coexistence of multiple autoignition kernels has been confirmed in Fig. 11, it is conceivable that homogenous autoignition (occurring at t = 0 to 0.5 ms in Fig. 8) is a potential explanation for this phenomenon.

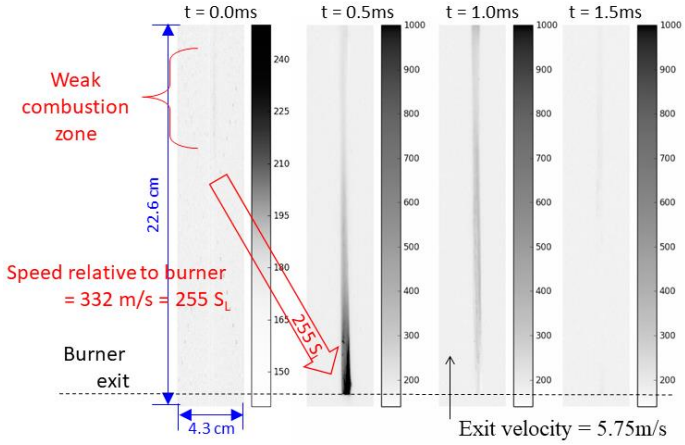

Fig. 13 Ultra-fast flashback

It is also possible these phenomena are coupled together. A typical result is illustrated in Fig.14 at the condition of U_0 = 2.37 m/s. This chemiluminescence signal is recorded directly using the high-speed camera at 4k frames per second. No intensifier or filter is used for this result. At t = 0 ms, the first detectable autoignition kernel (Kernel-1) is generated at approximately 11.5 cm downstream of the burner exit. This distance between the autoignition kernel and the nozzle exit is labeled as h_{ign}. 0.25 ms after that, a second autoignition (Kernel-2) is generated at the upstream of Kernel-1 (distance to the nozzle exit is approximately 7.0 cm). Both kernels start to grow and finally they merge. During t = 1.5 to 2 ms, the downstream part of this merged reacting zone burns out, while the upstream part evolves to a flame structure similar to a Bunsen flame. Finally, this flame propagates back to the nozzle exit.

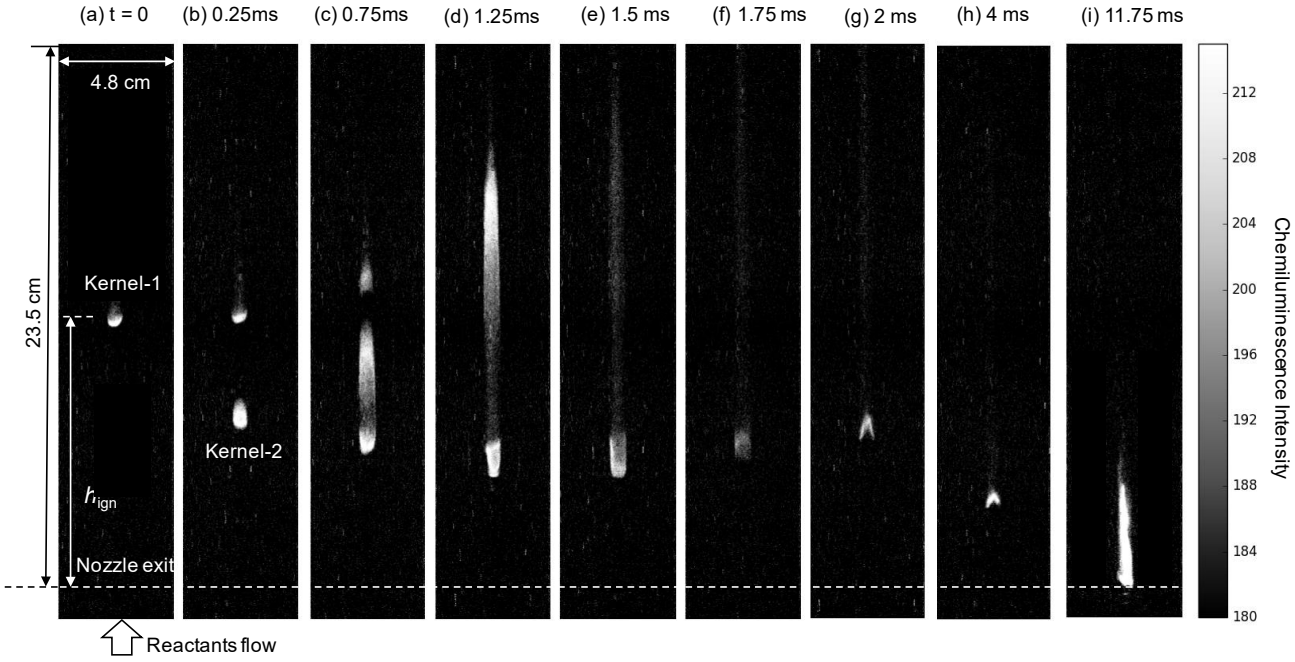

Fig. 14 Direct chemiluminescence from a flashback process

The reactants at this condition will not autoignite if no O_2 is converted to O_3, or if the fuel is replaced to one that has negligible ozonolysis reactions at room temperature such as CH_4. This confirmed that the autoignition kernel is activated by the explosive ozonolysis reactions of C_2H_4. Besides the autoignition, ozonolysis promotes the flashback of the reacting zone in several ways.

(i) During t = 0~0.25 ms, the co-existence of the multiple kernels shows a dynamically different with the conventional laminar jet flame theory. The generation of Kernel-2 effectively moved the height of the reacting zone front from 11.5 cm to 7.0 cm from t = 0 to 0.25 ms. This corresponds to a "propagation" speed of 180 m/s. This is more than 100 times of S_L. This dynamic with such extremely high "propagation" speed is controlled by autoignition. In contrast, the conventional laminar jet flame is controlled by flame propagation and the propagation speed is on the order of S_L.

(ii) During t = 0.25~1.25 ms, the propagation of front of the reacting zone is also extremely fast (~20 m/s). It is not likely to be a conventional flame propagation. In fact, the upstream reactants are already reacting prior to the front propagates upstream. Therefore, it's reasonable to expect that at upstream, reactive species already exist and temperature already rises. So, this propagation mechanism can be referred as "autoignition-assisted propagation". In contrast, the conventional flame propagation relies on the diffusion of the radicals and thermal energy. This difference may explain the extremely high propagation speed during this time.

To further investigate the role of ozonolysis reactions, a 1D simulation is conducted using adiabatic steady laminar plug flow reactor model (PLUG) [18]. It is predicted that autoignition occurs at 5.8 cm downstream, as shown in Fig. 15. This autoignition is a two-stage process. First stage ignition is activated by the ozonolysis reactions. Only when the temperature become sufficiently high (>800 K), the decomposition of O_3 (O_3+M=O_2+O+M) and other O_3 reactions become important. This again confirmed that the autoignition is activated by ozonolysis reactions. As a product of the

ozonolysis reactions, CH_2O is produced prior to the significant temperature rise. The peak mole fraction is approximately 1%. This implies it is possible to detect CH_2O chemiluminescence prior to the autoignition kernel is formed, or even at no-flame condition (e.g., when the reactants are diluted).

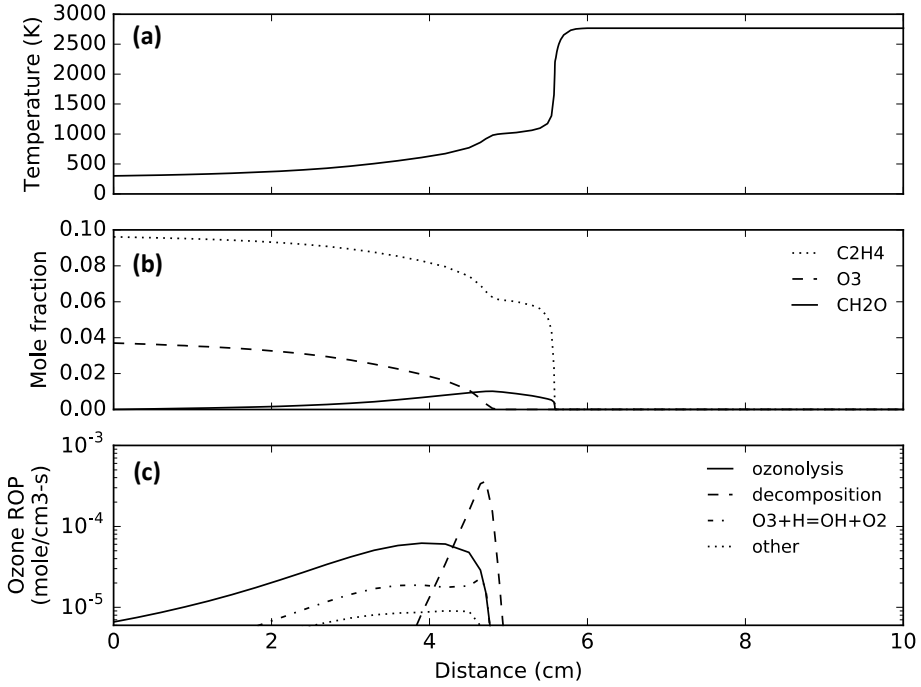

Fig. 15 Simulation results of PLUG model

To test the above implication about CH_2O, the experiment is repeated with an intensifier and a bandpass filter centered at 430 nm. This filter allows the chemiluminescence from both CH (a high-temperature species) and CH_2O (ozonolysis product at low temperature, as illustrated in Fig. 10(b)) to pass through. Typically, CH_2O chemiluminescence is not conducted because of the overlap of its chemiluminescence with that of CH and CH chemiluminescence is orders of magnitude stronger than CH_2O chemiluminescence. However, in our study, CH_2O is produced first from ozonolysis reactions without CH production. Therefore, CH_2O chemiluminescence could be measured. Images are taken at frame rate of 2.5 kHz and gate open time of 0.2 ms, and illustrated in Fig. 16. As in Fig.16(a~c), a weak emission zone is formed prior to high-intensity zone is formed. This is consistent with the expectation mentioned above that, CH_2O is generated prior to autoignition. It is worthy to mention that, once the autoignition kernel is formed, the front propagates back at a very high speed (~12 m/s) during t = 2~3.6 ms. This fast propagation stops at the location of upstream boundary of original CH_2O emission zone, which is consistent with the above-mentioned argument that, the reactive species generated and heat released from ozonolysis at upstream promotes the propagation and growth of the autoignition kernel.

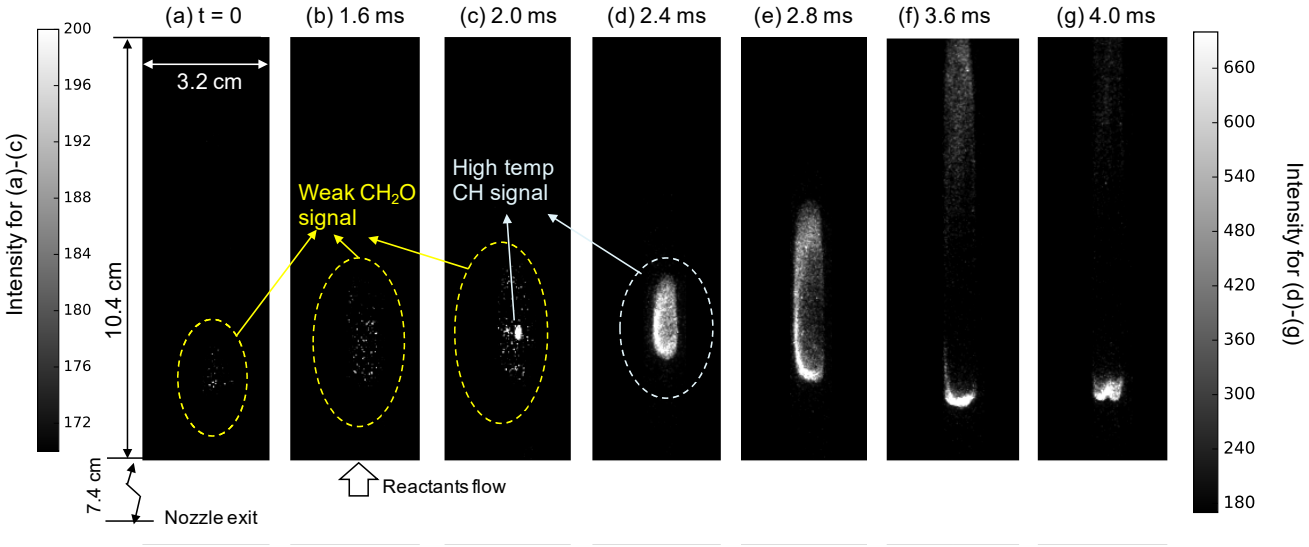

Fig. 16 Chemiluminescence passed through a 430 nm bandpass filter from an autoignition process

To further confirm that the weak emission in Fig. 16(a~c) is from CH_2O not CH, the reactants are diluted using N_2 to a no-flame condition. Temperature rise of ~150 K is measured at the exit of the quartz tube. Chemiluminescence signal (as shown in Fig. 17) is still observable at such condition. As CH is generally a high-temperature species and is not likely to appear at this no-flame condition, this chemiluminescence is from CH_2O, considering at this condition the only dominant reaction is ozonolysis and CH_2O is the one of its known product.

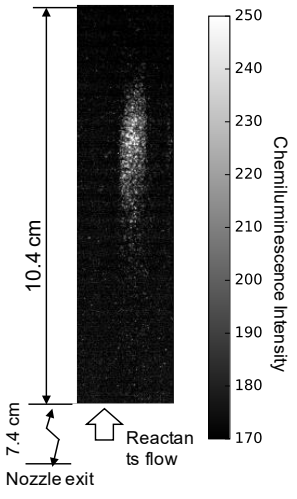

Fig. 17 Chemiluminescence passed through a 430 nm bandpass filter at no-flame condition

2.3. Numerical Simulation and Time Scale Analysis

This section provides the quantitative relation between the autoignition timescale and U_0. As the configuration is non-premixed, the mixing process is expected to be important to autoignition. To quantify this timescale, non-reacting fluid is simulated using FLUENT software [20]. The grid contains 40.5k nodes to ensure reasonably accurate results. The contour of the mixture fraction, Z, at the centerline slice is shown in Fig. 18. The stoichiometric iso-surface (calculated based on all

C, H, O atoms) is referred as $Z=Z_{st(all\ O)}$. The distance between the tip of this iso-surface and the nozzle exit is defined as the mixing distance, h_{mixing}. So, a mixing timescale can be defined as $\tau_{mixing} = h_{mixing}/U_0$. Unlike free jet, for the present setup, the width of the jet is constrained by the quartz tube. This promotes the mixing process and this effect is more obvious at higher U_0 as the jet becomes larger at higher U_0. As a result, τ_{mixing} decreases with U_0, as shown in Fig. 18.

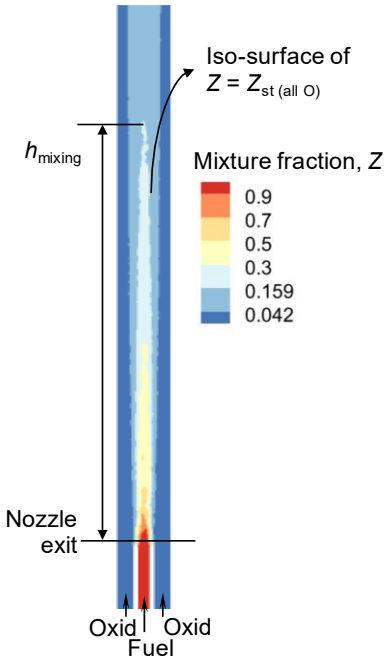

Fig. 18 Mixture fraction contour from non-reacting simulation results

Similarly, a timescale for the chemistry process can be defined as $\tau_{chem} = h_{PLUG}/U_0$. where h_{PLUG} is the axial location of the first point where temperature rise is greater than 1000 K. Unlike the mixing timescale, τ_{chem} remains constant as U_0 increases. Using the above-defined timescales for mixing and chemistry, a simplified model can be proposed for the autoignition timescale $\tau_{ign} = h_{ign}/U_0$

$$\tau_{ign} = \alpha\tau_{chem} + \beta\tau_{mixing}$$

where $\alpha>1$ is a parameter indicating the delay due to heat loss, and $\beta<1$ is a parameter indicating the reaction already starts at partially mixed condition. The optimized parameters to match the experimentally measured τ_{ign} are $\alpha = 1.5$ and $\beta = 0.65$, and the results are illustrated in Fig. 19. It successfully captured the trend that, for low U_0, τ_{ign} decreases with U_0, and this is due to the negative relation between τ_{mixing} and U_0 as discussed above. It is worthy to mention that, τ_{chem} and τ_{mixing} are on the similar order, this implies that the corresponding Damköhler number is on the order of 1, which is consistent with the argument that the studied combustion process is controlled by autoignition.

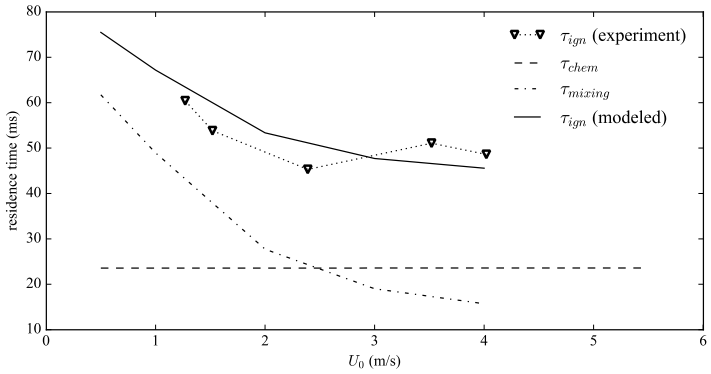

Fig. 19 Modeled and experimentally measured autoignition timescale

A more detailed FLUENT model can be built using reacting flow. To reduce the computational cost, a 5-step mechanism is proposed, as documented in Section 2.1. The validation is conducted for the autoignition process using a 0D adiabatic constant-pressure SENKIN model [19] at the conditions same to the experiment (initial temperature of 300 K, pressure of 1 atm, N/O ratio = 0.28, and 7.7% of O atoms exist in O_3). As the experiment configuration is non-premixed, the autoignition delay is compared at a wide range of ϕ (corresponding to different mixture fraction Z for the present fuel and oxidizer streams). As illustrated in Fig. 20(a), the detailed agree with the 5-step mechanism very well. The mixture fraction corresponding to the stoichiometric mixture for the ozonolysis (i.e., the ratio of C_2H_4 and O_3 is 1:1) is labeled as "stoich. (ozonolysis)"; the mixture fraction corresponding to the overall stoichiometric mixture (i.e., calculated considering all O atoms in both O_2 and O_3), is labeled as "stoich. (all O)" and corresponds to $\phi = 0.4$; the mixture fraction corresponding well-mixed fuel/oxidizer stream is labeled as "overall". This 5-step mechanism is also able to two-stage ignition process, as illustrated in Fig. 20(b) for $\phi = 0.4$.

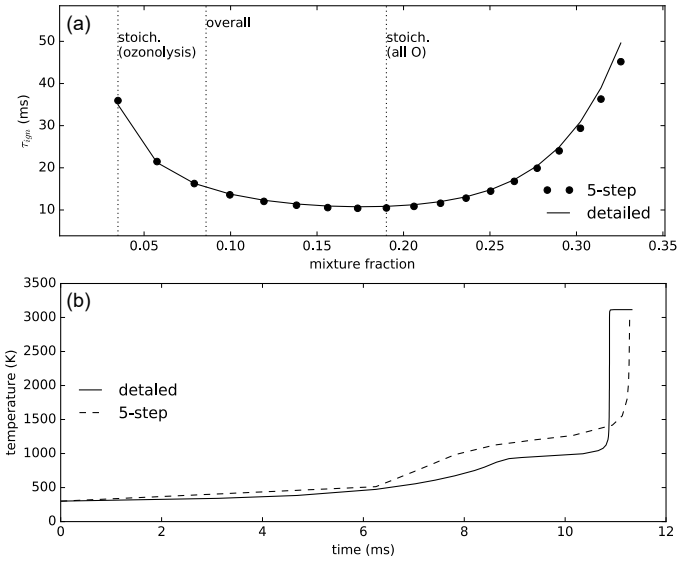

Fig. 20 Validation of the 5-step mechanism (a) autoignition delay at varying mixture fractions, (b) autoignition process

Applied this mechanism, transient simulation is conducted using FLUENT. The same geometry grid as in the previous section is applied. Similar to the experiment procedure, initially the fluid

field is full of oxidizer. The wall for the fuel tube is assumed to be isothermal (temperature fixed at 300 K) as in experiment this wall is stainless steel and conducts thermal energy rapidly. The outer wall is assumed to be adiabatic as the quartz tube in experiment is not highly thermally conductive. The simulation is able to predict some transient phenomenon observed in the experiment. For example, the accumulation of CH_2O prior to autoignition is illustrated in Fig. 21. At t = 0, the maximum temperature is only 831 K but a CH_2O region has been formed. 2 ms after, a hot spot is formed in the CH_2O region and the maximum temperature goes up to 2068 K. This is consistent with the experimentally observed process shown in Fig. 16(a~c).

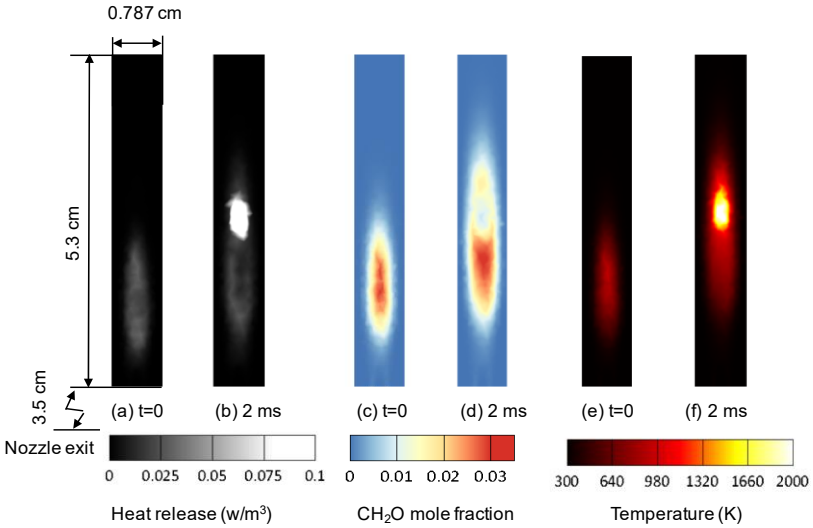

Fig. 21 Simulation of the generation of autoignition kernels

After the autoignition kernel is formed, it grows and two heat release regions are formed, shown in Fig. 22(b). The downstream part then burns out, consistent with the process experimentally observed in Fig. 16(d~g).

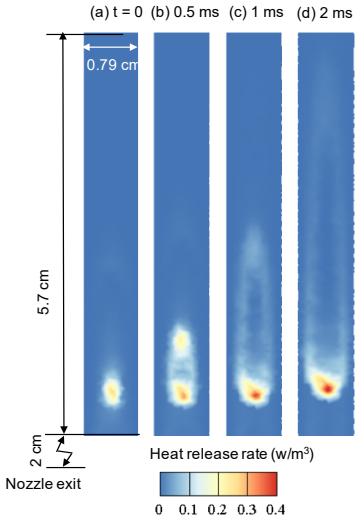

Fig. 22 Simulation of the splitting and burn out of autoignition kernels

This simulation also predicts the relation between τ_{ign} and U_0 more accurately, as shown in Fig. 23. The non-monotonic relation is successfully captured. However, τ_{ign} is underestimated. This may result from heat loss and mechanism inaccuracy in the simulation model.

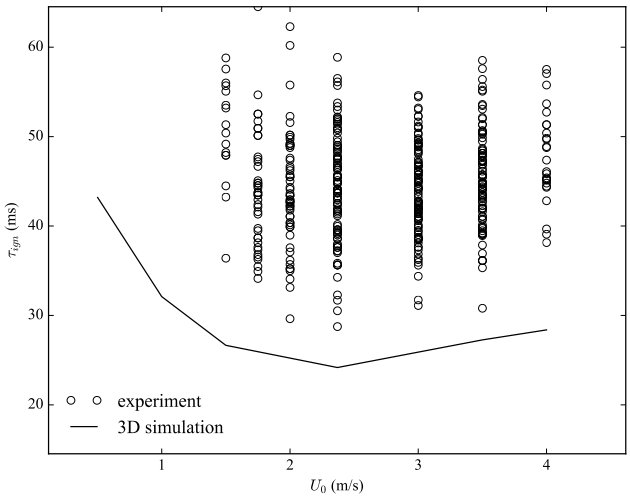

Fig. 23 Simulated experimentally measured autoignition timescale

2.4. Effect of turbulence on autoignition

The experimental observation above indicates that the height where autoignition kernel occurs is controlled by mixing in the shear layer. Ozonolysis reactions cannot occur until center fuel jet is mixed with oxidizer co-flow. In this study, the Reynolds number (Re) of the bulk flow only ranges from ~500 to 3000. It is still in the range of unsteady laminar region. It is expected that with the increase of Re, turbulence can significantly enhance the mixing in the shear layer therefore decrease the height where first autoignition kernel occurs. In order to study the effect of turbulence, preliminary study was conducted by placing metal mesh in the co-flow tube to create turbulence. The measured heights of autoignition kernel with and without artificial turbulence are shown in Fig. 24. It can be clearly seen that turbulence enhances mixing in the shear layer therefore promoting ozonolysis reactions to result in faster autoignition. By examining the measurement, it can also be seen that autoignition delays decrease much faster in the case with metal mesh.

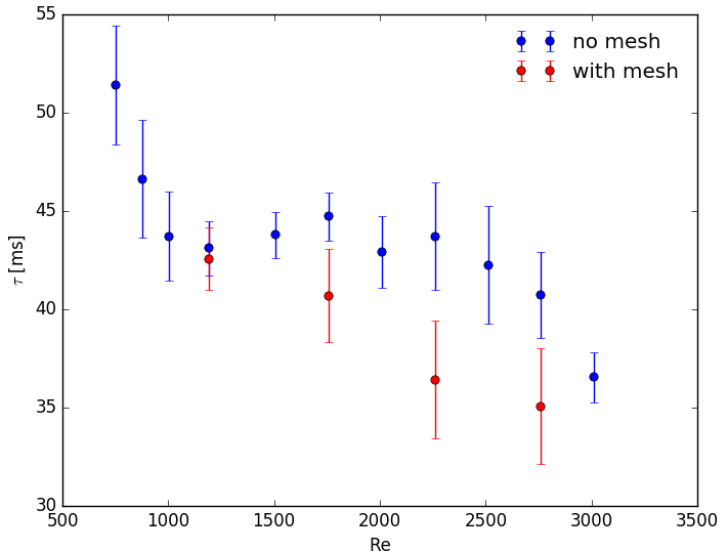

Fig. 24 relationship between Re and autoignition delays (converted from height of autoignition kernel) with and without metal mesh in co-flow tube

3. Task 3 – Investigation the effect of ozonolysis reactions on flame dynamics

This task is to investigate the effect of ozonolysis reactions at room temperature on flame dynamics. We conducted experiments using lifted flame at steady state to understand how the reactions at mixing layer change the dynamics of flame.

3.1. Experimental Method

Figure 25 shows the schematic of experiment setup. The lifted flame burner consists of a central fuel nozzle with 1.3 mm inner diameter. The lifted flame burner consisted of a central fuel jet with an inner diameter of 0.271 mm that was located in a 90 mm inner diameter fused silica (quartz) tube to contain the co-flow of oxidizer. The fuel nozzle was aerodynamically shaped to produce a uniform velocity profile at the exit. The large ratio of diameters between the oxidizer co-flow and the fuel jet (>100) were used. To ensure that the co-flow was uniform, two stainless steel meshes coated with silica for chemical inertness were separated by 3 cm and were located between the oxidizer inlet of the burner and the fuel jet exit. The gases used in the experiments were C_2H_4 for the fuel and ultra-high purity O_2 (99.99%) and N_2 (99.95%) mixed for the oxidizer. Through the experiments, the flow velocity of oxidizer (co-flow) was fixed as 0.014 m/s and the composition of oxidizer co-flow is O_2/N_2 = 13/87. To change the lift off height, C_2H_4 flow velocity was either 3.29 m/s or 4.5 m/s. The higher the flow velocity, the larger the liftoff height. Figure 26 shows the direct photographs of lifted flames at different fuel jet velocities without O_3 addition. The distribution of CH_2O is qualitatively characterized by PLIF employing the 3rd harmonic Nd:YAG laser at 355 nm, and a 0.5 mm thick, 28 mm width laser sheet is formed by the combination of a concave lens and two convex lenses. Fluorescence signal of CH_2O corresponding to $\tilde{A}^1A_2 \rightarrow \tilde{X}^1A_1$ transition is collected by a high-speed camera (NAC GX-3) coupled with an intensifier (Video Scope International Ultracam3) with a 425 nm centered band-pass filter. To track flames at different stable positions, a periscope system is used to accurately adjust the laser sheet along the axial direct of the burner. During the experiments, 400 images are accumulated in each measurement and background scattering is subtracted to increase the signal-to-noise ratio.

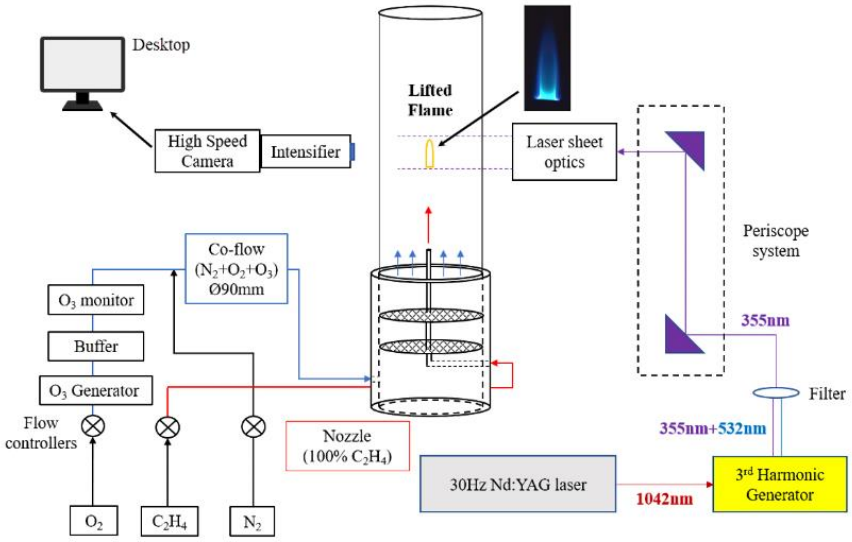

Fig. 25 Schematic of experimental setup

Fig. 26 Direct photographs of lifted flame with fuel jet velocities at 3.29 m/s and 4.5 m/s without ozone addition

3.2. Computational framework

Numerical simulations are performed using FLUENT with SIMPLE algorithm. Axisymmetric 2-D computational domain is adopted with 450 mm in axial and 45 mm in radial directions. A gravitational acceleration of 9.79 m/s^2 is given in the negative axial direction so that buoyancy effect could be counted. The build-in CHEMKIN-CFD solver with laminar finite-rate chemistry is enabled. Detailed USC Mech II model [24] is firstly reduced (for shorter computational time) and then input as the gas-phase kinetic model. The model reduction is conducted using Global Pathway Selection (GPS) algorithm [23]. The resulting skeletal kinetic model contains 43 species compared to 111 species in the detailed model with maximum deviation on autoignition delay and flame speed predictions of approximately 4.5 % and 4.9 %, respectively. In the kinetic model, the ozonolysis reaction of C_2H_4/O_3 is described by a 4-channel model, assuming equal reaction rate constants of each reaction channel. The four reaction channels are listed in Table S1 in the supplementary material together with other key O_3 relevant reactions adopted from Ref. [25]. This ozone kinetic model was employed in previous studies [22, 26] and qualitative agreements were reported between numerical and experimental results. It should be advised that reproduce of detailed reaction scheme of ozonolysis is extremely challenging. Stabilized Criegee Intermediate (sCI) [27] is not included in this model. The reactions in Table S1 are incorporated into the reduced USC Mech II model for simulation.

3.3. Results

With fuel jet velocity fixed at 3.29 m/s, ozone was added into the co-flow and with the change of ozone concentration, the liftoff height changed as shown in Fig. 27. It can be seen that with the increase of ozone concentration, the liftoff height decreased. However, if the initial liftoff height was relative higher with fuel jet velocity fixed at 4.5 m/s, the liftoff height increased with the increase of ozone concentration. The results are shown in Fig. 28.

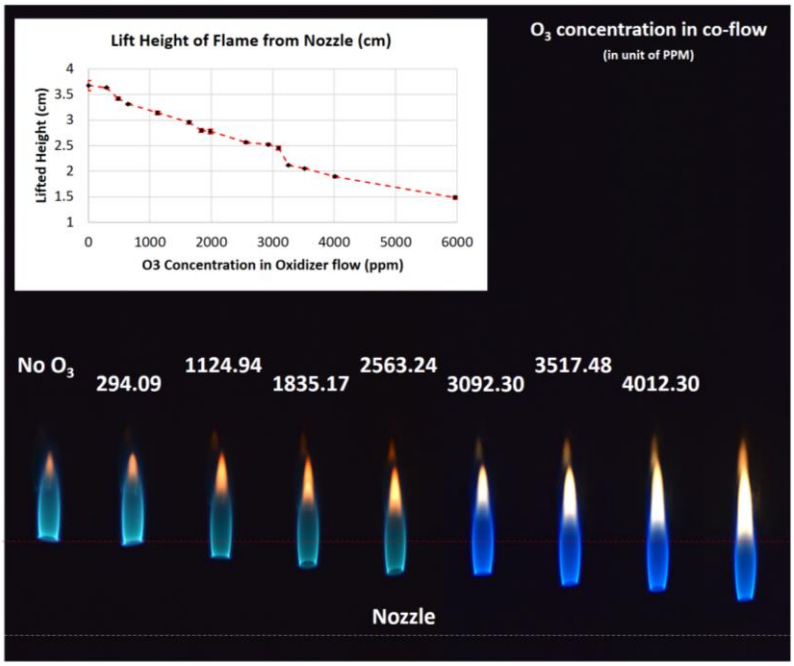

Fig. 27 Change of lift off height in terms of ozone concentration with fuel jet velocity 3.29 m/s

Starting from the fuel nozzle exit, C_2H_4 starts to mix with oxidizer and a mixing layer is formed. Once ozone is added into the co-flow, ozone starts to react with C_2H_4 immediately. There exist two competing reaction pathways, ozonolysis and ozone decomposition. Ozonolysis reactions produce significant amount of CH_2O and release heat. However, ozone decomposition is only significant at flame front at elevated temperature condition. To confirm the occurrence of ozonolysis reactions, CH_2O PLIF was conducted using 30Hz Nd:YAG laser at 355 nm. The schematic of the PLIF system is also shown in Fig. 25. Figure 29 shows CH_2O PLIF measurement with and without O_3 addition at low initial liftoff height condition. It can be seen clearly that with the increase of ozone concentration in co-flow, CH_2O concentration increased. However, with low liftoff height, there was not enough time for ozonolysis to proceed before the reactants reaching the flame front. Therefore, O_3 decomposition will dominate in the overall effect of ozone addition. Ozone decomposition can accelerate flame propagation speed, therefore decrease the liftoff height of lifted flame.

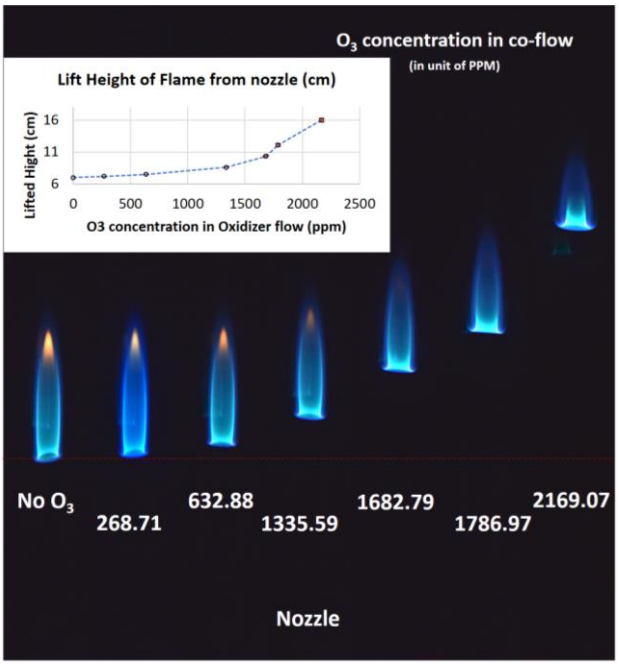

Fig. 28 Change of lift off height in terms of ozone concentration with fuel jet velocity 4.5 m/s

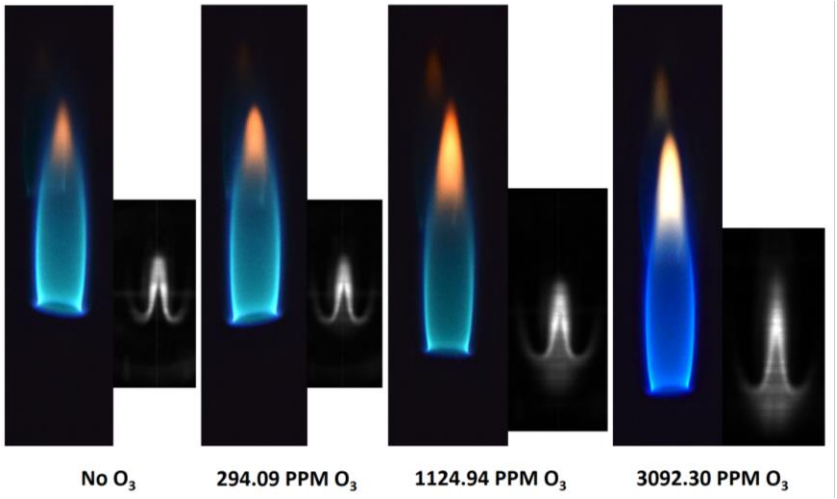

Fig. 29 Direct photograph (left) and CH_2O PLIF (right) with and with ozone with fuel jet velocity at 3.29 m/s

If the initial liftoff height is high, longer resident time is given for ozonolysis reactions to proceed before the reactants reaching the flame front. Therefore, ozonolysis reactions will dominate in the overall effect of ozone addition. Figure 30 shows the CH_2O PLIF and direct photograph of the flame with 921 ppm ozone addition in the co-flow.

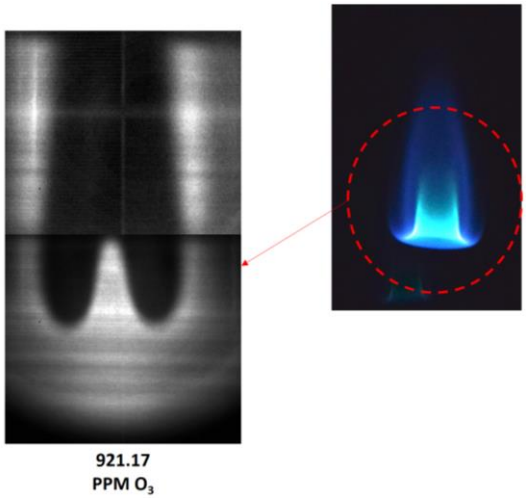

Fig. 30 CH_2O PLIF (left) and direct photograph (right) with 921 ppm ozone addition with fuel jet velocity at 4.5 m/s

To understand the effect of ozonolysis reaction on flame dynamics, systematic experiments on stable C_2H_4 laminar lifted flames are conducted with pure fuel jet and O_2/N_2 mixture co-flow at different fuel jet velocities (u_f). Figure 31 shows direct photographs of C_2H_4 lifted flame at different u_f but constant co-flow velocity, U_{CO} = 0.013 m/s, and constant composition as 12.7% O_2 + 87.3% N_2.

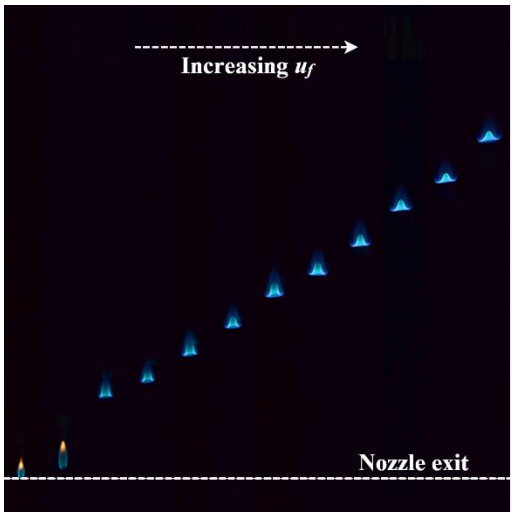

Figure 31. Direct photographs of steady lifted flame with nozzle exit d = 0.69 mm

As the flame is lifted, clear triple flame structure appears with a relatively weak lean premixed wing and strong rich premixed wing, and the tailing diffusion flame in between, intersecting at the so-call triple point. For steady lifted flame, dynamic balance between u_{st} and S_{tri} must be satisfied at the corresponding H_L as $u_{st} = S_{tri}$. The triple point locates on the stoichiometric contour where fuel mass fraction $Y_F = Y_{F,st}$ (the stoichiometry mass fraction $Y_{F,st}$ is calculated with C_2H_4 as fuel and corresponding O_2/N_2 co-flow mixture as oxidizer). Non-reacting flow simulations are performed and comparison between numerically simulated stoichiometric contours, in terms of

axial (x_{st}) and radial position (r_{st}), and experimental triple points locations is shown in Fig. 32. The simulated $Y_{F,st}$ contours and experimental measurements agree reasonably well.

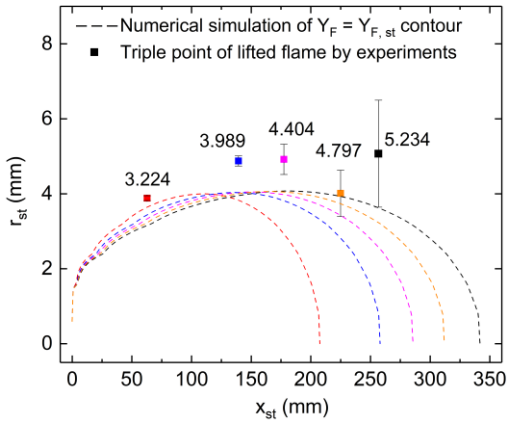

Figure 32. Comparison of numerical simulations (dash line) and experimental triple point positions (solid point). Different jet velocities u_f are referred by colors

To study the effect of O_3 addition on lifted flame dynamics, a stable lifted C_2H_4 flame is first established and then ozone generator is turned on to convert part of O_2 into O_3. All lifted flame experiments presented here are performed with co-flow composition of 11.5% O_2 + 88.5% N_2 and U_{CO} = 0.016 m/s. Figure 33(a) shows the liftoff heights of flames with the different of O_3 additions in co-flow. It is interesting that with the same O_3 addition in the co-flow, opposite trend on the change of H_L can be observed. The lifted flame descends with O_3 addition if u_f is small or equivalently initial liftoff height ($H_{L,0}$) is low, while ascends instead if the initial value of u_f is relatively large. At high $H_{L,0}$ condition, e.g. with u_f = 3.68 m/s, the addition of O_3 above 150 ppm results in flame blow-out.

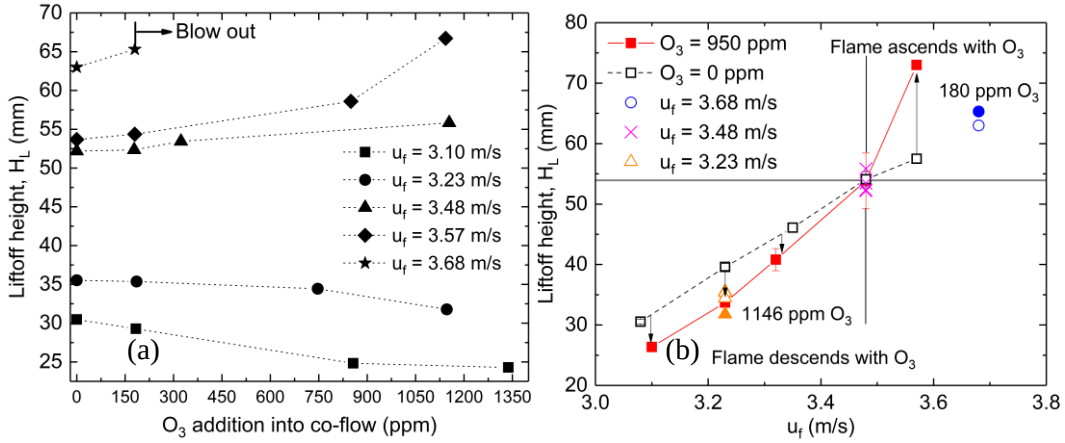

Figure 33. Relationship of liftoff height with (a) increasing O_3 addition in co-flow at different fuel jet velocities and (b) ranging u_f of constant O_3 in co-flow

Further experiments are conducted with different u_f but constant O_3 concentration in the co-flow, and the measured liftoff heights are shown in Fig. 33(b). Noticeable change in H_L can be seen at both relatively low and high $H_{L,0}$ while the effect of O_3 addition on H_L diminishes at $H_{L,0}$ in between. Therefore, the effect of O_3 addition on lifted C_2H_4 flame is a function of $H_{L,0}$ (or

equivalently u_f). As the fuel jet velocity increases, O_3 addition would firstly decrease and then increase H_L. Based on the observed two-way phenomenon with O_3 addition on flame liftoff height, competing pathways must exist.

As one of the main products of ozonolysis reaction, CH_2O is considered as indicator of ozonolysis reaction. CH_2O PLIF measurement is then conducted for lifted flames with and without O_3 addition. Figure 34 shows overlaid images of CH_2O PLIF and broadband chemiluminescence collected by the same ICCD camera at (a) u_f = 3.10 m/s and (b) u_f = 3.57 m/s correspond to cases of $\Delta H_L < 0$ and $\Delta H_L > 0$, respectively. Gray value of CH_2O PLIF is sampled at horizontal level of the triple points of each lifted flame as illustrated in Fig. 34 as well. For both cases with no O_3 addition, CH_2O is only detected at premixed wings of the triple flames. Once O_3 is added, scattered CH_2O fluorescence starts to appear upstream. As O_3 concentration keeps increasing, more intense fluorescence signals are recorded. By moving the laser sheet upstream, it is found that CH_2O starts to form near the nozzle exit where C_2H_4 and O_3 starts to mix in the shear layer.

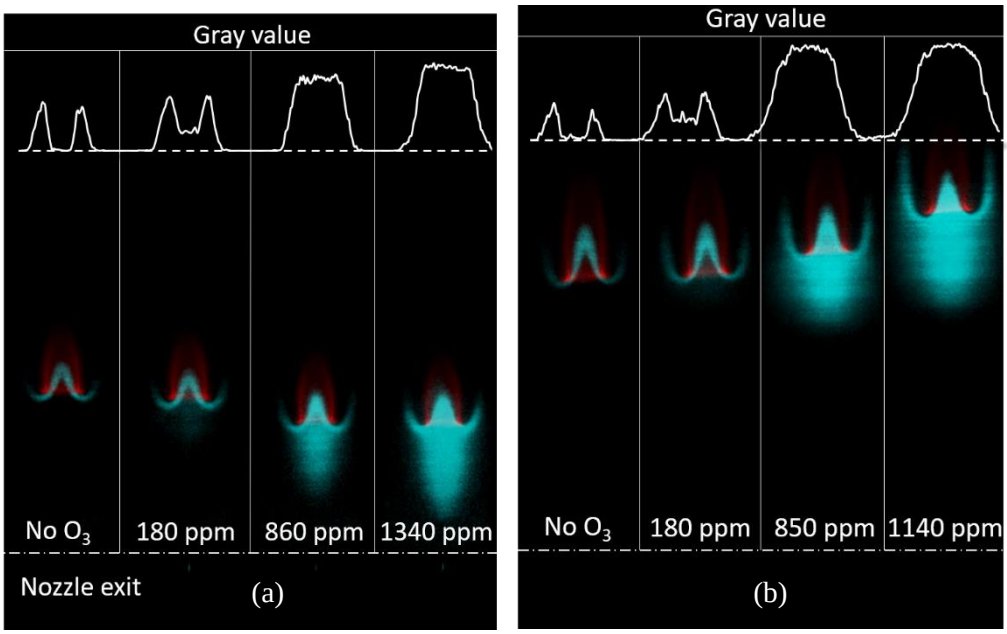

Figure 34. CH_2O PLIF of lifted flames with (a) u_f = 3.10 m/s and (b) u_f = 3.57 m/s

CH_2O PLIF measurements show that ozonolysis reaction proceeds far upstream of the flame regardless of the value of initial liftoff height. Now the questions are that why the two-way competing phenomenon of the change of liftoff height is observed even if ozonolysis always occurs regardless and what is the underlying kinetic/dynamic process. To answer these questions, numerical simulations are performed.

The effect of O_3 addition on laminar flame speed, S_L therefore S_{tri}, is evaluated using CHEMKIN [28]. A 1-D Plug Flow Reactor (PFR) model is connected in tandem with Premixed Laminar Flame Speed Calculator to mimic the effect of C_2H_4 ozonolysis reaction upstream. The residence time in PFR is set to be τ_{PFR} = 20 ms, which is approximately the same as the value estimated from the nozzle exit to the bottom of the lifted flame, $\tau \sim H_L/u_f$. Energy equation is solved in PFR model with adiabatic boundary and inlet condition T = 298 K and P = 101 kPa. The fuel is C_2H_4 and oxidizer is $O_2/O_3/N_2$ mixture and stoichiometry is unity. Calculations are conducted at different τ_{PFR} so that cases with both low and high $H_{L,0}$ can be compared. S_L is also calculated with O_3 addition while the ozonolysis reaction is turned off but other O_3 related

reactions remain the same. Results are presented in Fig. 35. It is clearly shown that considerable enhancement in S_L should be expected with O_3 addition. Furthermore, approximately 0.84% increment on S_L is obtained if ozonolysis reaction is included compared to the case without ozonolysis reaction at 2000 ppm O_3 addition and τ_{PFR} = 20 ms. Nevertheless, the overall enhancement in S_L owing to O_3 addition should be expected at both low and high $H_{L,0}$, which should result in increase of S_{tri} and liftoff height should decrease regardless of its initial value. However, the change in chemical composition caused by ozonolysis reaction should also be considered on the effect of flame dynamics.

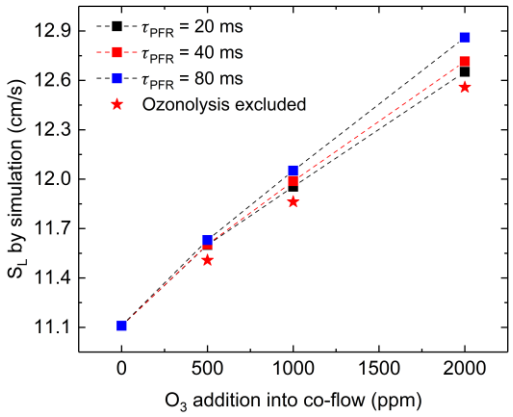

Figure 35. Calculated S_L with different amount of O_3 addition using a PFR + Laminar Flame Speed model

Xue et al. [29] investigated liftoff characteristic of dimethyl ether (DME) flame and no stable lifted DME jet flame could be observed. The observation was rationalized by the much larger $Y_{F,st}$ of DME comparing to hydrocarbon fuels, which consequently renders a much higher u_{st} for DME according to the linear relation between $Y_{F,st}$ and u_{st} predicted by Landau-Squire similarity solution [30, 31]. Analogically, it is indicating that u_{st} and $Y_{F,st}$ can be significantly affected owing to the change in chemical composition caused by ozonolysis reaction upstream of the flame. Ozonolysis reaction yields large amount of CH_2O which blends with C_2H_4, and thus the fuel stream transits to C_2H_4/CH_2O mixture gradually. Calculation of $Y_{F,st}$ indicates that 10% of CH_2O transition of C_2H_4 results in 7.6% increase in $Y_{F,st}$, so as the u_{st}. The increase in S_{tri} and u_{st} results in decrease and increase of flame liftoff height, respectively, and these two effects compete with each other. Therefore, at low $H_{L,0}$ condition, the effect from S_{tri} surpasses that from u_{st}, therefore flame liftoff height decreases. At high $H_{L,0}$ condition, higher yield of CH_2O (owing to longer residence time) could further increase u_{st} and consequently liftoff height increases.

Qualitative FLUENT simulations are further performed with lifted flames established firstly at both low and high liftoff heights, respectively, then 2000 ppm O_3 is added. The CH_2O distribution before and after O_3 addition are presented in Fig. 36. With O_3 addition, the lifted flame in the high $H_{L,0}$ case starts to move downstream and eventually blow-out occurs, while for the low $H_{L,0}$ case, the position of lifted flame remains nearly unchanged. The stoichiometric C_2H_4 mass fraction contour $Y_{F,st}$ is indicated by red lines in Fig. 36. It can be seen that the stoichiometry contour becomes thinner after O_3 addition, indicating a higher u_{st}. Figure 37(a) and (b) show the results of u_{st} and local CH_2O mole fraction, respectively, along the $Y_{F,st}$ contour.

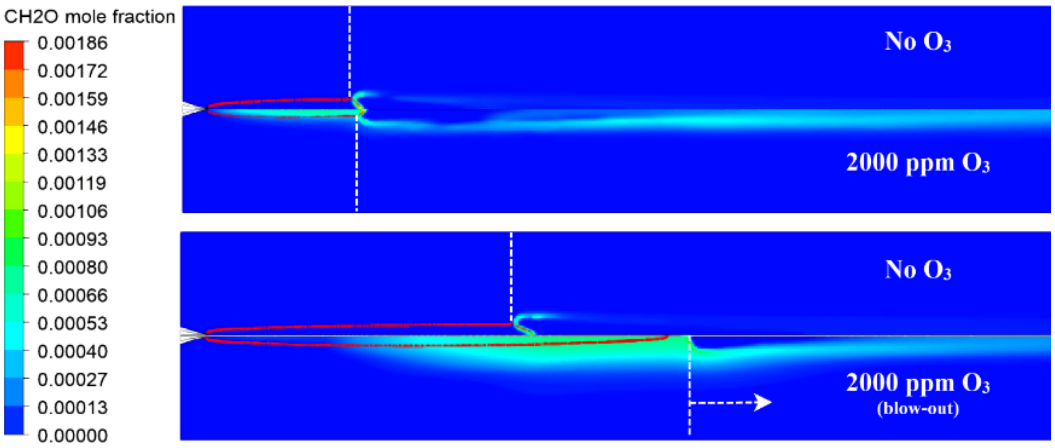

Figure 36. FLUENT simulation of CH_2O distribution before and after O_3 addition

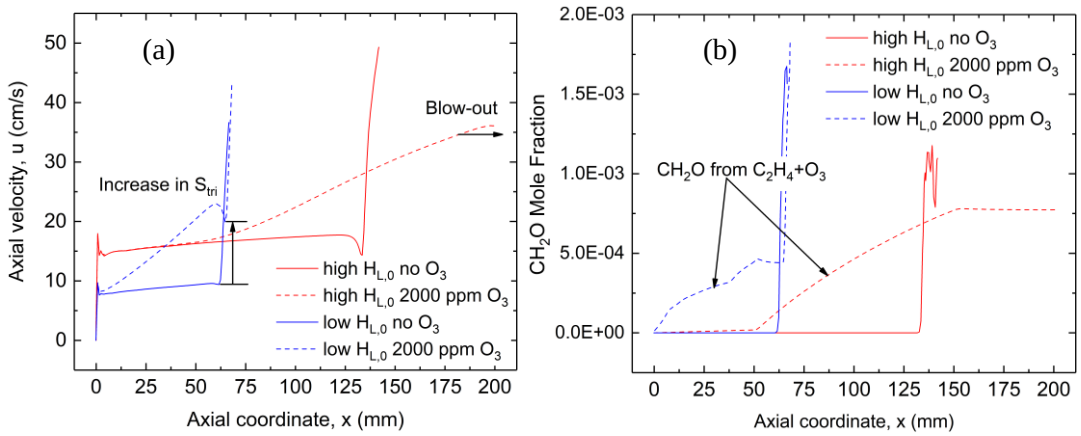

Figure 37. Results along $Y_{F,st}$ contour with and without O_3 addition of (a) u_{st} and (b) CH_2O mole fraction

For the high $H_{L,0}$ case, it is demonstrated in Fig. 37(a) and 37(b) that O_3 addition results in continuous increase of CH_2O as well as u_{st} along the stoichiometry contour. However, the increase of u_{st} is very dramatic that the increasing S_{tri} could not balance with it, and consequently the flame moves downstream and eventually blows out. For low $H_{L,0}$ case, the steady lifted flame with O_3 addition directly indicates a nearly doubled S_{tri} through $u_{st} = S_{tri}$. The increase on S_{tri} cancels out with the increase of u_{st}, and lifted flame remains.

4. Publications and Presentations

Journal papers:

[1]. B. Wu, M. Hasting, W. Sun, T. Ombrello, C. Carter, "Dynamics of laminar ethylene lifted flame with ozone addition," 2019 (submitted)

[2]. W. Sun, X. Gao, B. Wu, T. Ombrello, "Ozone assisted combustion: Dynamics and chemistry" 2019 ***Progress in Energy and Combustion Science***, 73, 1-25

[3]. X. Gao, B. Wu, W. Sun, T. Ombrello, C. Carter, "Ozonolysis activated autoignition in non-premixed coflow", 2019 ***Journal of Physics D: Applied Physics***, 52(10), 105201

[4]. Choe, Jinhoon, and Wenting Sun. "Blowoff hysteresis, flame morphology and the effect of plasma in a swirling flow." ***Journal of Physics D: Applied Physics*** 51.36 (2018): 365201.

[5]. Li, He-Ping, Kostya Ken Ostrikov, and Wenting Sun. "The energy tree: Non-equilibrium energy transfer in collision-dominated plasmas." ***Physics Reports*** (2018). 770-772, 1-45 (IF=20)

[6]. S. Yang, S. Nagaraja, W. Sun, V. Yang, "Multiscale modeling and general theory of non-equilibrium plasma-assisted ignition and combustion", ***Journal of Physics D,*** 2017 50 433001

Conference papers:

[1]. B. Wu, X. Gao, W. Sun, "Investigation of ethylene ozonolysis reaction rate constant at room temperature and pressure" Technical Meeting of Eastern States Section of the Combustion Institute, State College, PA, March 4-7, 2018

[2]. B. Wu, X. Gao, W. Sun, "The Investigation of Ozonolysis Reactions of Ethylene at Combustion Environment Using a Flow Reactor" *53rd AIAA/SAE/ASEE Joint Propulsion Conference*, Atlanta, GA, July 10-12, 2017

[3]. X. Gao, S. Yang, B. Wu, W. Sun, "The effects of ozonolysis activated autoignition on non-premixed jet flame dynamics: a numerical and experimental study" *53rd AIAA/SAE/ASEE Joint Propulsion Conference*, Atlanta, GA, July 10-12, 2017

[4]. X. Gao, W. Sun, T. Ombrello, C. Carter, "The Effect of Ozonolysis Activated Autoignition on Jet Flame Dynamics" *10th U. S. National Combustion Meeting*, College Park, MD, April 23-26, 2017

[5]. X. Gao, W. Sun, T. Ombrello, C. Carter, "The effect of ozonolysis activated autoignition on jet flame dynamics" *AIAA 55th Aerospace Science Meeting*, Grapevine, TX, January 9-13, 2017

Invited talks:

[6]. "The effect of explosive ozonolysis reaction on jet flame stabilization" Keynote lecture, the 6th Aerospace Thematic Workshop on Fundamentals of Plasma Assisted Combustion and Flow Control, St. Petersburg, Russia, April 2017

4. Reference

[1] Fenske JD, Hasson AS, Paulson SE, Kuwata KT, Ho A, Houk KN. The pressure dependence of the OH radical yield from ozone-alkene reactions. J Phys Chem A. 2000;104:7821-33.
[2] Criegee R. Mechanism of ozonolysis. Angewandte Chemie International Edition in English. 1975;14:745-52.
[3] Lias S. Ionization energy evaluation. NIST chemistry webbook, NIST standard reference database. 2005;69.
[4] Cool TA, Wang J, Nakajima K, Taatjes CA, Mcllroy A. Photoionization cross sections for reaction intermediates in hydrocarbon combustion. International Journal of Mass Spectrometry. 2005;247:18-27.
[5] Holmes J, Lossing F, Terlouw J, Burgers P. The radical cation [CH2OH2]+. cntdot. and related stable gas-phase ion-dipole complexes. Journal of the American Chemical Society. 1982;104:2931-2.

[6] Cool TA, Nakajima K, Mostefaoui TA, Qi F, McIlroy A, Westmoreland PR, et al. Selective detection of isomers with photoionization mass spectrometry for studies of hydrocarbon flame chemistry. The Journal of chemical physics. 2003;119:8356-65.
[7] Rousso AC, Hansen N, Jasper AW, Ju Y. Low-Temperature Oxidation of Ethylene by Ozone in a Jet-Stirred Reactor. The Journal of Physical Chemistry A. 2018;122:8674-85.
[8] Womack CC, Martin-Drumel M-A, Brown GG, Field RW, McCarthy MC. Observation of the simplest Criegee intermediate CH2OO in the gas-phase ozonolysis of ethylene. Science advances. 2015;1:e1400105.
[9] Battin-Leclerc F, Herbinet O, Glaude PA, Fournet R, Zhou Z, Deng L, et al. Experimental Confirmation of the Low-Temperature Oxidation Scheme of Alkanes. Angewandte Chemie International Edition. 2010;49:3169-72.
[10] Meloni G, Zou P, Klippenstein SJ, Ahmed M, Leone SR, Taatjes CA, et al. Energy-resolved photoionization of alkylperoxy radicals and the stability of their cations. Journal of the American Chemical Society. 2006;128:13559-67.
[11] Albrecht B, Allan M, Haselbach E, Neuhaus L, Carrupt PA. Molecular-Ions of Transient Species - Vinyl-Alcohol Cation. Helv Chim Acta. 1984;67:216-9.
[12] Schubert CC, Schubert S, Pease RN. The Oxidation of Lower Paraffin Hydrocarbons. I. Room Temperature Reaction of Methane, Propane, n-Butane and Isobutane with Ozonized Oxygen1. Journal of the American Chemical Society. 1956;78:2044-8.
[13] Morrissey RJ, Schubert C. The reactions of ozone with propane and ethane. Combustion and Flame. 1963;7:263-8.
[14] DeMore WB, Sander SP, Golden DM, Hampson RF, Kurylo MJ, Howard CJ, et al. Chemical Kinetic and Photochemical Data for Use in Stratospheric Modeling: Evaluation No. 11 of the NASA Panel for Data Evaluation. JPL Publication 94-26. 1994.
[15] Atkinson R, Baulch DL, Cox RA, Crowley JN, Hampson RF, Jr., Kerr JA, et al. Summary of Evaluated Kinetic and Photochemical Data for Atmospheric Chemistry. IUPAC Subcommittee on Gas Kinetic Data Evaluation for Atmospheric Chemistry. 2001;Web Version December 2001.
[16] Shi Y, Xu Y, Jia L. Arrhenius parameters for the gas-phase reactions of O3 with two butenes and two methyl-substituted butenes over the temperature range of 295–351 K. Int J Chem Kinet. 2011;43:238-46.
[17] Kee RJ, Grcar JF, Smooke M, Miller J, Meeks E. PREMIX: a Fortran program for modeling steady laminar one-dimensional premixed flames. 1985.
[18] Larson RS. PLUG: A Fortran program for the analysis of plug flow reactors with gas-phase and surface chemistry. Sandia Labs., Livermore, CA (United States); 1996.
[19] Lutz AE, Kee RJ, Miller JA. SENKIN: A FORTRAN program for predicting homogeneous gas phase chemical kinetics with sensitivity analysis. Sandia National Labs., Livermore, CA (USA); 1988.
[20] FLUENT release 17.1. ANSYS, Inc. 2016.
[21] Wang H, You X, Joshi AV, Davis SG, Laskin A, Egolfopoulos F, et al. USC mech version II. High-temperature combustion reaction model of H. 2007;2.
[22] Gao X, Zhang Y, Adusumilli S, Seitzman J, Sun W, Ombrello T, et al. The effect of ozone addition on laminar flame speed. Combustion and Flame. 2015;162:3914-24.
[23] Gao X, Yang S, Sun W. A global pathway selection algorithm for the reduction of detailed chemical kinetic mechanisms. Combustion and Flame. 2016;167:238-47.
[24] Wang H, You X, Joshi AV, Davis SG, Laskin A, Egolfopoulos F, et al. USC Mech Version II. High-Temperature Combustion Reaction Model of H2/CO/C1-C4 Compounds. 2007.
[25] Wang ZH, Yang L, Li B, Li ZS, Sun ZW, Aldén M, et al. Investigation of combustion enhancement by ozone additive in CH4/air flames using direct laminar burning velocity measurements and kinetic simulations. Combustion and Flame. 2012;159:120-9.
[26] Gao X, Wu B, Sun W, Ombrello T, Carter C. Ozonolysis activated autoignition in non-premixed coflow. Journal of Physics D: Applied Physics. 2019;52:105201.
[27] Alam MS, Camredon M, Rickard AR, Carr T, Wyche KP, Hornsby KE, et al. Total radical yields from tropospheric ethene ozonolysis. Physical Chemistry Chemical Physics. 2011;13:11002-15.

[28] Kee RJ, Rupley FM, Miller JA. Chemkin-II: A Fortran chemical kinetics package for the analysis of gas-phase chemical kinetics. Sandia National Labs., Livermore, CA (USA); 1989.
[29] Xue Y, Ju Y. Studies on the liftoff properties of dimethyl ether jet diffusion flames. Combustion science and technology. 2006;178:2219-47.
[30] Landau L. New exact solution of the Navier-Stokes equations. Doklady Akad Nauk SSSR1944. p. 311-4.
[31] Squire HB. The round laminar jet. The Quarterly Journal of Mechanics and Applied Mathematics. 1951;4:321-9.